Marine Geology 459 (2023) 107032

Contents lists available at ScienceDirect

Marine Geology

journal homepage: www.elsevier.com/locate/margo

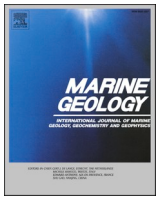

Research Article

A multi-proxy approach to assess tsunami hazard with a preliminary risk assessment: A case study of the Makran Coast, Pakistan

Rashid Haider [a,d,*], Sajid Ali [b], Gösta Hoffmann [c], Klaus Reicherter [a]

[a] Institute of Neotectonics and Natural Hazards, RWTHAachen University, Lochnerstr. 4-20, 52056 Aachen, Germany
[b] COMSATS University Islamabad, Abbottabad campus, Department of Earth sciences, Pakistan
[c] UNESCO Global Geoparks Unit, Department Heritage, Nature, Society, German Commission for UNESCO, Martin-Luther-Allee 42, 53175 Bonn, Germany
[d] Geoscience Advanced Research Laboratories, Geological Survey of Pakistan, Islamabad 45500, Pakistan

ARTICLE INFO

Editor: Edward Anthony

Keywords:
Tsunami hazard
Inundation analysis
Makran subduction zone (MSZ)
Multi-proxy approach

ABSTRACT

Tsunamis and cyclones are sea-borne hazards capable of inundating vast coastal areas. This study aims at an extreme wave hazard assessment with a preliminary inundation analysis along the Makran Coast, Pakistan. The coastal hazard, particularly tsunamis, is evaluated by integrating five approaches: (i) probabilistic tsunami hazard assessment (PTHA); (ii) deterministic tsunami hazard assessment (DTHA); (iii) geophysical-seismic (2-D thermal modelling), (iv) sedimentary tsunami deposits (tsunamis); and (v) the historical record. The recurrence interval for a mega-tsunami event (≥12 m) is between 500 and 1000 years in the Arabian Sea. Of these mega-tsunamis, about 60% are generated by seismic sources, while the remaining 40% are attributed to secondary (co-seismic submarine landslides) and other non-seismic sources. Based on the above five approaches, the hazard analysis helped to shortlist four wave scenarios (3, 7, 10, and 15 m). Which were further used to demarcate risk areas through static inundation analysis. The results indicated that the damage potential at the coast is minor to negligible with 3 m waves and moderate with 7 m waves. Whereas the 10 m and 15 m waves will severely disrupt the study area. In addition to tsunami risk, cyclone risk is assessed by interpolating storm tracks dating back to 1842 CE. In the last 64 years, cyclone frequency has jumped from 1 cyclone per 10 years to 20 cyclones per 10 years, and the intensity has increased by two levels from Tropical Storm (TS) to Category-3.

1. Introduction and aims

Tsunamis, cyclones and rising sea levels are natural hazards to coastal areas. In the Indian Ocean, the 1970 Bhola cyclone in the Bay of Bengal, the 1998 Gujarat cyclone in the Arabian Sea, and the 2004 tsunami along Sumatra Island are some of the major catastrophic events that resulted in >0.8 million casualties and more than USD 14 billion in property loss (Frank and Husain, 1971; Kalsi and Gupta, 2003; Bell, 2011). In spite of such huge losses, the lessons learned from these events are not widely anticipated on the mitigation side (Løvholt, 2017). In this regard, the Makran Coast of Pakistan is also poorly prepared, as the life and property losses during the 1945 tsunami and the cyclones of 1998, 1999, 2007, 2010 and 2021 reflect a dejected level of preparedness and resilience. Along the coastline of Pakistan, >24 million people are exposed to these hazards (see Fig. 1). Another point of concern is the Karachi Nuclear Power Plant (KANUPP) at the coast near Karachi, which may create a cascading catastrophe similar to the 2011 Fukushima Daiichi nuclear disaster by releasing radioactive material in the ocean and atmosphere.

The historic record of cyclones and tsunamis along the coast is perplexing due to the scarcity of historical records and the palaeo-dynamics of extreme wave events, which impedes hazard assessment. Further, the study area lacks field investigations for the palaeo-extreme wave events to approximate their recurrence intervals and coastal impacts. Significant exploratory work has been carried out along Oman's neighbouring coastlines. (Donato et al., 2008, 2009; Pilarczyk et al., 2011; Hoffmann et al., 2011, 2013a,b, 2014, 2015, 2020; Hoffmann and Reicherter, 2014; Koster et al., 2014), Iran (Shah-Hosseini et al., 2011; Vaziri et al., 2016) and India (Sangode and Meshram, 2013; Bhatt et al., 2016; Gandhi et al., 2017; Prizomwala et al., 2015, 2018, 2021, 2022), where sedimentary deposits (tsunamites) from extreme wave events are reported. These pieces of evidence suggest that the northern Arabian coastline was repeatedly hit by extreme waves. These extreme events are mostly attributed to the tectonic and climatic settings of the region.

* Corresponding author at: Institute of Neotectonics and Natural Hazards, RWTH Aachen University, Lochnerstr. 4-20, 52056 Aachen, Germany.
E-mail address: r.haider@nug.rwth-aachen.de (R. Haider).

https://doi.org/10.1016/j.margeo.2023.107032
Received 8 December 2022; Received in revised form 2 March 2023; Accepted 22 March 2023
Available online 24 March 2023

From a tectonic perspective, the Makran Coast is highly susceptible to tsunamis and the Makran Subduction Zone (MSZ) is the main source of tsunamigenic earthquakes. Since 1945, the Coast has witnessed two tsunamigenic earthquakes; a major one in 1945 (Mw 8.1) claiming some hundred human lives (Pendse, 1946; Hoffmann et al., 2013a, 2013b) and a minor tsunami in 2013 (Mw 7.7) with no losses (Heidarzadeh and Satake, 2014b).

So far, at the Makran Coast, either a deterministic or probabilistic approach is used to assess the tsunami hazard. The probabilistic approach is considered mature (Behrens et al., 2021) due to the advantage of equating the contribution of possible small and large events and of treating different sources of uncertainty (El-Hussain et al., 2018). On the other hand, the deterministic approach considers a specific scenario that involves various components, including (i) source type and its parametrization; (ii) modelling tsunami generation and its propagation in shallow and deep ocean; and (iii) simulation of coastal inundation (Heidarzadeh et al., 2009b). For coastal engineering, a deterministic approach is considered more useful as it allows the derivation of the worst-case scenario (max. Wave height, inundation extent and depth) to design an engineering structure and also avoids the complications associated with probabilistic analysis. For near field tsunamis, the problems with these approaches are associated with large data gaps, the maximum hazard potential and its spatial distribution. Furthermore, the former approach also entails knowledge gaps, assumptions and uncertainties. Also, there is no single accepted way of defining the worst-case scenario. Multidisciplinary and multiproxy approaches improve hazard and risk assessment (Koshimura et al., 2014; De Martini et al., 2021; Röbke et al., 2015, 2016, 2018). Regarding integrated analysis, the Makran Coast probabilistic and deterministic approaches are integrated for hazard and risk assessment by (Khan et al., 2003a, 2003b; Salmanidou et al., 2019; Rashidi et al., 2020; Yang et al., 2022). Here, we compiled and integrated five different approaches (geophysical, sedimentological-geomorphic, probabilistic modelling, numerical modelling and historical record), which we called a synergic approach for hazard assessment. As each approach has its own limitations, the synergic analysis provides better outcomes and a higher level of confidence. A key tool for coastal risk assessment is the use of inundation maps. Few studies on inundation analysis have been conducted as Heidarzadeh et al. (2009a, 2009b) created inundation models for the cities of Pasni and Karachi using 100 m topographic resolution and 12 m wave height. Mahmood et al. (2012) modelled Gwadar for a 3.7 m high wave on the 90 m topography of the Shuttle Radar Topography Mission (SRTM). Surface topography with a resolution of at least 25 m is considered suitable for inundation analysis and evacuation planning (Griffin et al., 2015). The resolution of topography used in both cases is too coarse for risk assessment. In this study, 12 m topography is used for inundation analysis with four different wave heights (3, 7, 10, 15 m) for the cities of Karachi, Gwadar, Pasni and Ormara. The outcomes are presented as maps delineating the areas at risk. The objective of the paper is to assess the maximum tsunami hazard potential at the Makran Coast through a multiproxy approach as discussed above. Further, based on the hazard potential, areas vulnerable to extreme waves are demarcated in four major cities.

2. Study area

2.1. Geodynamics

The geodynamics of the study area is evolving from the interaction of three tectonic plates: the Eurasian, Indian, and Arabian plates (see

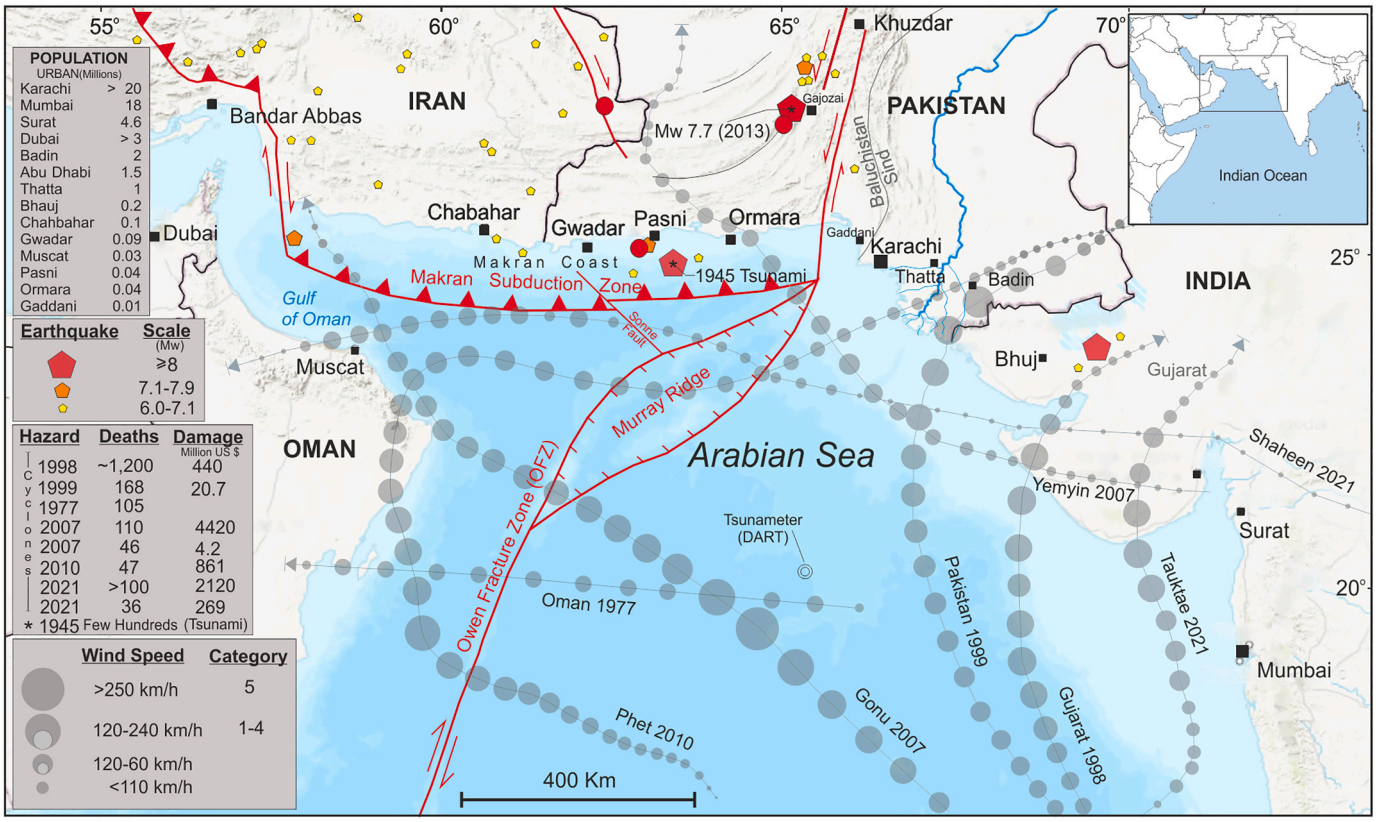

Fig. 1. Location map showing the regional plate tectonic setting (red) and the major cyclones tracks (grey) which hit the coasts in the Arabian Sea. The size of the grey circle on the cyclone's tracks corresponds to the Saffir-Simpson Hurricane Scale. Data sources: International Best Track Archive for Climate Stewardship-IBTrACS (Knapp et al., 2010). Earthquake data: International Seismological Centre (ISC-2020). (For interpretation of the references to colour in this figure legend, the reader is referred to the web version of this article.)

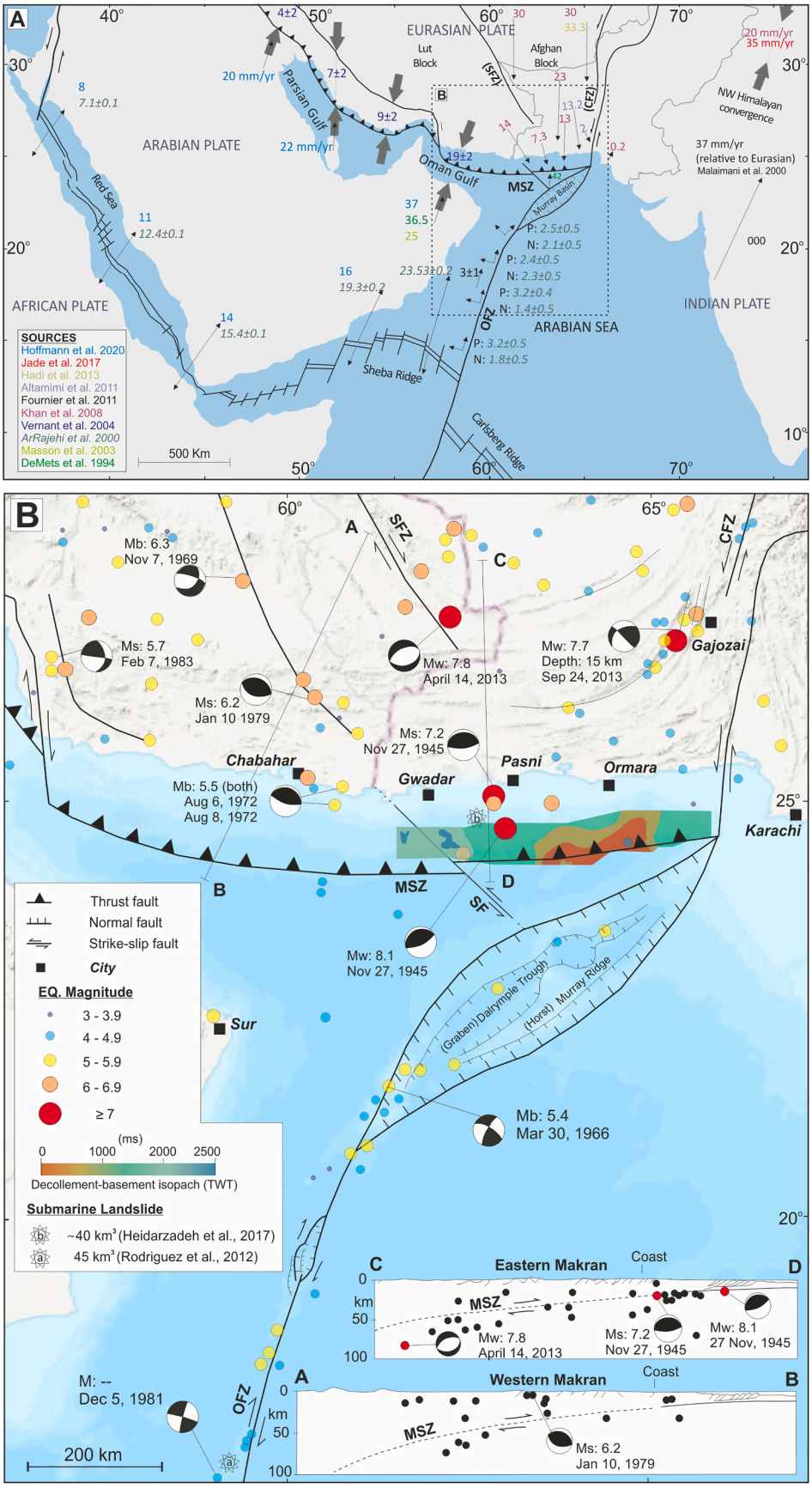

Fig. 2. A: Figure showing the tectonic setting and the geodetic motions of the study area. All the velocity vectors are in millimetres (mm). Black Arrows (thin): Speed vector, P: perpendicular vector, N: normal vector, grey arrows (thick): convergence vectors. Different numbers against the vectors show reporting by different researchers, as indicated by different colours in the legend. Makran Subduction Zone (MSZ), Chaman-Ornach Nal Fault Zone (CFZ), Owen Fracture Zone (OFZ), Sistan Fault Zone (SFZ), Sonne Fault (SF).
B: Seismo-tectonic map of the region Earthquake focal mechanisms are compiled from Quittmeyer and Kafka (1984); Gordon and Demets (1989); Byrne et al. (1992); Fournier et al. (2001). The simplified two-way travel time (TWT) map is from Smith et al., (2012) showing the nature of the horizon between the decollement and basement. The cross-sections are integrated from Byrne et al. (1992).

Fig. 2). The Eurasian plate is further segmented into micro plates, known as "blocks." Similarly, the Arabian Plate also has a submarine microplate known as the Ormara plate (Kukowski et al., 2000). The tectonic accommodation between these plates is complex and depends on the crust type at the converging fronts, the relative speed and the direction of plate motion. Plate interactions are variable, but along some boundaries certain patterns can be observed (see Fig. 2A).

The rate of spreading at the mid-oceanic ridge (Red Sea) gradually increases from 7.1 ± 5.0 mm at the north to 23.53 ± 0.2 mm to the south at Sheba Ride (ArRajehi et al., 2010). This pattern of divergence is likewise accommodated at the Makran and Zagros subduction zones with average dipping of 3 degrees (Kopp et al., 2000), 2 degree (White and Louden, 1982). The convergence rate increases from 4 ± 2 mm in the Persian Gulf to 19 ± 2 mm in the Gulf of Oman (Vernant et al., 2004). The plate dynamics at the eastern part of the MSZ are anomalous, as the GPS velocity at the Pasni Coast is about half the speed of its eastern and western parts (Khan et al., 2008), which reflects a partial locking or the high-friction subduction zone. The Arabian Plate forms transform boundary with the Indian Plate with a relative motion of 3 ± 1 mm/y (Reilinger et al., 2006; Fournier et al., 2008; Rodriguez et al., 2011).

2.2. Seismicity

Submarine earthquakes have triggered around 80% of the total tsunami events documented globally (Harbitz et al., 2014; Løvholt, 2017). The remaining 20% are caused by landslides, volcanos and meteoric impacts in water bodies (Behrens et al., 2021). Overall, the study area is moderately seismic, but events like the 1945 tsunamigenic earthquake (Mw: 8.1) have created uncertainty. The seismicity along the MSZ is not uniformly distributed; the western part of the MSZ (offshore Iran) is relatively silent as compared with its eastern part (offshore Pakistan). The silence in the western Makran indicates either aseismic subduction or the interlocking of plate boundaries, which can generate great earthquakes with long recurrence intervals (Byrne et al., 1992). Geodetic measurements show 19.5 mm/y convergence (Vernant et al., 2004), therefore it is not locked (see Fig. 2). The Eastern MSZ is seismically active and most of this activity is attributed to the Sonne Fault (Kukowski et al., 2000). Smith et al. (2013) relates this seismicity to the nature of the decollement. The decollement in the south-west of Pasni is brittle as indicated by high seismic velocities (<4.4 km/s). The brittle behaviour is due to the absence of soft sediments (very thin or zero) in contrast to its western part. The velocities of these sediments are comparable to those observed at depth in the December 2004 Sumatra rupture area. The thermal modelling of MSZ shows that it has a potential to trigger an Mw 9.2 earthquake (Smith et al., 2013). Another thermal modelling study shows its potential as Mw 8.65 ± 0.26 and 8.75 ± 0.26 in western (Iran) and eastern (Pakistan) Makran respectively (Khaledzadeh and Ghods, 2022). Regarding the 1945 tsunamigenic earthquake (Mw: 8.1), Laane and Chen (1989) through P-wave first motion studies suggested that the event has a large component of normal faulting instead and proposed a lithospheric normal faulting event usually associated with down-going slabs of old age. In contrast, the detailed studies on the focal mechanism of the 1945 Makran earthquake by Byrne et al. (1992) show that it is related to a thrust event. Their dislocation models, body waveform inversion and moment estimates indicate that the earthquake ruptured 100 to 200 km of crust along the arc in a down-dip direction. The Murray Ridge has been the easternmost region of small earthquakes due to right-lateral strike-slip and normal faulting (Banghar and Syke, 1981). Quittmeyer et al. (1979) confine the seismicity only along its north-eastern half. The seismicity along the OFZ is also low to moderate, the maximum magnitude recorded is Mw 5.8 earthquake (Rodriguez et al., 2011).

2.3. Submarine landslide potential

An underwater landslide has the potential to displace a large amount of water, which generates a set of waves formally known as a tsunami (Heidarzadeh and Satake, 2017; Röbke et al., 2018; Latcharote et al., 2018; Salmanidou et al., 2019). Mostly, under normal conditions, loose submarine sediments can withstand an angle of 12^{o}-30^{o} (Salaree and Okal, 2015) but other factors, especially seismic shaking can trigger a landslide with even lower steepness. The Arabian Sea has a considerable potential for the huge offshore landslides due to a 7 km-thick sedimentary sequence in the Makran Accretionary Prism (MAP) (White and Louden, 1982) and a ~ 500 m thick pelagic drape on Owen Ridge (Shipboard Scientific Party, 1989). The high erosion rate is interpreted for these thick sequences (Kukowski et al., 2001; Ellouz et al., 2007).

The tsunamis of 1945 and 2013 are the most recent examples from the study area, which have been hypothesised to have been generated by offshore landslides (Heidarzadeh and Satake, 2014a, 2014b; Hoffmann et al., 2014). In the 1945 tsunami, there was a 3 h delay between the earthquake and the first tsunami wave at Pasni, situated at about 40 km from the epicenter (Pendse, 1946). To explain this delay, Yanagisawa et al. (2009) through inverse numerical modelling argued for a 3 h delay due to multi-wave reflection and amplification phenomena. Heidarzadeh and Satake (2017) simulated three possible secondary sources (splay faulting, delayed ruptures, and submarine landslides) and proposed that only a submarine landslide having a volume of ~40 km3 (see Fig. 2B) can reproduce the near-field tsunami of 1945 at Pasni and Karachi.

On the bathymetric map of MAP, Kukowski et al. (2001) and Ellouz et al. (2007) identified many circular and linear slump scars. Grando and McClay (2007) interpreted slumping phenomena on the seismic lines. Slumping at MAP is generally noticed on the frontal, south-dipping folded limb, where the thrust faults propagated by folds have achieved significant height and relief. Mouchot et al. (2010) suggested that in this active setting, slope instabilities seem frequent but limited in size. Platt et al. (1985) attributes the slumping and the very rough morphology of the upper slope to the active uplift and actual tension. The mass movements ultimately settle in the deeper parts as turbidites. The age of the Late Quaternary turbidite sequence (sedimentary cores) and earthquake record show a good correlation (Prins et al., 2000; Bourget et al., 2010).

Along the Owen Ridge, Fournier et al. (2011) and Rodriguez et al. (2012, 2013) mapped the several types of giant mass failures along the western side of Owen Ridge by using the multibeam bathymetry and sediment echo-sounder. Southern Owen Ridge displays the largest failure area and the most voluminous landslides and the highest estimated volume of activated material during a landslide is up to 45 km3 (see Fig. 2B). Their research shows that the mass-wasting frequency is low due to the chaotic nature and slow sedimentation rate, but earthquakes are more frequent, implying that mass failures are severely limited by sedimentation rates. In the eastern most part, the landslide potential of the Indus Delta is the least studied. The Indus River prior to modern damming used to supply at least 250 Mt./year to the Arabian Sea (Milliman and Syvitski, 1992), other estimates emphasise a larger range of 100 to 675 Mt./year (Ali and De-Boer, 2008). Since the last glaciation, the Indus River has shed about 4050–5675 km3 of sediment into the Arabian Sea and about half of the stored sediments lie offshore on the shelf and in the submarine Indus canyon (Clift and Giosan, 2014). The massive accumulation of sediments in the offshore and canyon areas makes the delta vulnerable to landslides and necessitates further investigation.

2.4. Cyclones

In the Arabian Sea, tropical storms, also called cyclones, mostly develop either before the monsoon (May–June) or after the monsoon (October–November) with an almost equal ratio. Cyclones form when

the temperature of the surface water rises above 25 °C, preferably between 28 and 29 °C (V. K. Singh and Roxy, 2022). The rising temperature develops a low-pressure region (961 hPa in the 1998 Gujarat Cyclone), which drifts laterally. The cyclones preferentially develop over the south-eastern quadrant of the Arabian Sea and sometimes a few of these develop in the Bay of Bengal and in their course of landfall, they gradually turn into depressions or well-marked low-pressure areas, but as they approach the Arabian Sea, they intensify into new cyclones. The cyclones Shaheen 2021 and Yemyin 2007 in the Arabian Sea developed from the remnants of Gulab Cyclone and Deep Depression BOB 03/2007, respectively, in the Bay of Bengal. In the Arabian Sea, the Coriolis force sometimes recurves the cyclone track clockwise towards the northwestern coast of India and Pakistan (Pedgley, 1967).

3. Methodology and data

Multidisciplinary and multiproxy approaches improve hazard and risk assessment (Koshimura et al., 2014; De Martini et al., 2021; Röbke et al., 2013, Röbke et al., 2015, 2016, 2018). At the Makran Coast, PTHA and DTHA are used together by (Khan et al., 2003a, 2003b; El-Hussain et al., 2018; Salmanidou et al., 2019; Yang et al., 2022; Zafarani et al., 2022). We compiled and integrated five different approaches (geophysical, PTHA, DTHA, sedimentary tsunami deposits, and historical record), which we called a synergic approach for hazard and risk assessment. The data and workflow are summarised in Table 1 and Fig. 3, respectively. The problems with PTHA and DTHA are associated with large data gaps, maximum hazard potential determination, spatial distribution, assumed and uncertain variables and different computational types (Berryman, 2005; Behrens et al., 2021). To improve hazard assessment, the PTHA (see Fig. 5) and DTHA (see Table 2) results are compared with the more meticulously evaluated seismic hazard potential (PGA), which includes weightage from the area's tectonic elements and recurrence intervals. Further, analysis of the recurrence interval is improved by the compilation and correlation of historical records (see Table 3 in the supplements) and tsunamites records discovered at different sites around the Arabian Sea (see Table 5). For these tsunami deposits, MSZ is inferred as the tsunami source except for one mentioned in the table.

To assess the maximum wave potential, the tsunamites record of 1000 CE is taken as the worst-case discovered so far. This worst-case attribution is due to its high frequency in Table 5 and its far-flung spatial distribution (eastern and south-eastern Indian and Omani Coasts), which reflect that the event was not local but regional and of a high scale. The tsunami boulder deposits at Fins-Sur, Oman, are up to 40 tons for which an approximate wave velocity of 4.5–6.6 m/s is calculated for dislodging, uplift and transport (Hoffmann et al., 2013a, 2013b) with maximum run-up height of ≥17 m (Koster et al., 2014). The numerical inundation modelling of wave velocities for Mw 9.0 is between 7 and 11 m/s by Mahmood et al. (2012). The deterministic slip models for Mw 9.0 earthquake, TSUNAMI-N2, MIKE 21 FM, COMCOT by Heidarzadeh et al. (2009a, 2009b), Payande et al. (2014), Rashidi et al. (2018a, 2018b) can produce a maximum amplitude of 15 m, 18 m and 23 m respectively. Two studies on the thermal modelling of decollement; Mw 9.2 and Mw 8.7 by Smith et al. (2013) and Khaledzadeh and Ghods, (2022) respectively support the Mw 9.0 earthquake mechanism hypothesis. The probabilistic models are finally considered, the tsunamis probability of ≥12 m is 0.6 in 5000 years (Hoechner et al., 2016) but as of Zafarani et al. (2022) it is 0.8 in 2475 years. The probable PGA value of 1.0 with a return period of 2500 years capable of generating a Mw 8.0 earthquake (Ahmed et al., 2019; Waseem et al., 2019, 2020) is in close agreement with the Zafarani et al. (2022) model. The results of Khan et al. (2003a, 2003b) are entirely different as they calculated the recurrence interval for this much intensity as 70 years, as the well-known historical record of the last 300 years does not account for such an interval.

The second part of the study includes a preliminary inundation analysis based on the evaluated hazard index. For inundation studies, cyclones are another source to be considered. The cyclone hazard map in the Arabian Sea is produced through interpolation of the historical cyclone record since 1842. The data is available from the International Best Track Archive for Climate Stewardship (IBTrACS), 2021. The entire region is classified into five hazard indices based on track density using natural neighbour interpolation. The cyclones are categorised according to the Saffir-Simpson Scale, which is based on the central pressure and the wind speed. A research gap exists in storm surge modelling along the Makran Coast. However, the wavelength of tsunamis is much larger and more devastating as compared with storm surges. For crude estimation, the maximum storm surge heights of some historic cyclones in the Arabian Sea are compiled in Table 4 (supplements).

Using the bathtub approach, flow depths are computed by inundation height and local topography difference. The method assumes a maximum uniform wave run-up consistent with tsunamites recorded along the shoreline and floods the base level connected to the beach. The approach, in sometimes modified versions, is used to study the tsunami risk assessment in Tohoku, Japan (Masuda et al., 2012); Akoli, Greece (Tarbotton et al., 2012); Samoa, Pacific (Smart et al., 2016); Muscat, Oman (Schneider et al., 2016); Augusta, Italy (Pagnoni et al., 2021; Williams et al., 2021). The static bathtub approach is modified in two

Table 1
Approaches, methodologies and data used.

	Approach	Methodology/ Model	Data/ Reference
Cyclone hazard	Probabilistic	Map based on cyclone density tracks	IBTrACS, (1842–2021)
Seismic hazard	Probabilistic	Poissonian model, (Cornell and Vanmarcke, 1969)	Khan et al. (2003a, 2003b)
		Cornell–McGuire (1968–1976)	Waseem et al. (2019, 2020)
		UBC 97 (International Conference of Building Officials, 1997)	Ahmed et al. (2019)
	Deterministic	Ambraseys and Boomer (1991) Model	Khan et al. (2003a, 2003b)
	Probabilistic	Synthetic tsunami-EQ catalogue spanning over 3 million years	Hoechner et al. (2016)
		Logic tree technique	Zafarani et al. (2022)
Tsunami hazard	Deterministic	Tsunami triggered by faults and landslide-based parameters	Compiled: 50 deterministic tsunami models (Table 2)
	Historical Tsunami	Makran historical and instrumental great earthquakes with Mw ≥ 6.5	Updated after Heidarzadeh et al. (2008)
	Tsunamites Record	Compilation of tsunamites discovered at different coasts along the Arabian Sea	Compiled: 14 studies/ 8 inferred tsunamites
Risk assessment	Bathtub Approach	Tohoku, Japan (Masuda et al., 2012) Akoli, Greece (Tarbotton et al., 2012) Samoa, Pacific (Smart et al., 2016) Muscat, Oman (Schneider et al., 2016) Augusta, Italy (Pagnoni et al., 2021; Williams et al., 2021)	· DEM: TanDEM-X 0.4 arcsec (12 m) · Land use: Google Earth-ESRI imagery, Open Street Maps (OSM), and the city survey & planning maps · Statistics Bureau of Pakistan, 2017

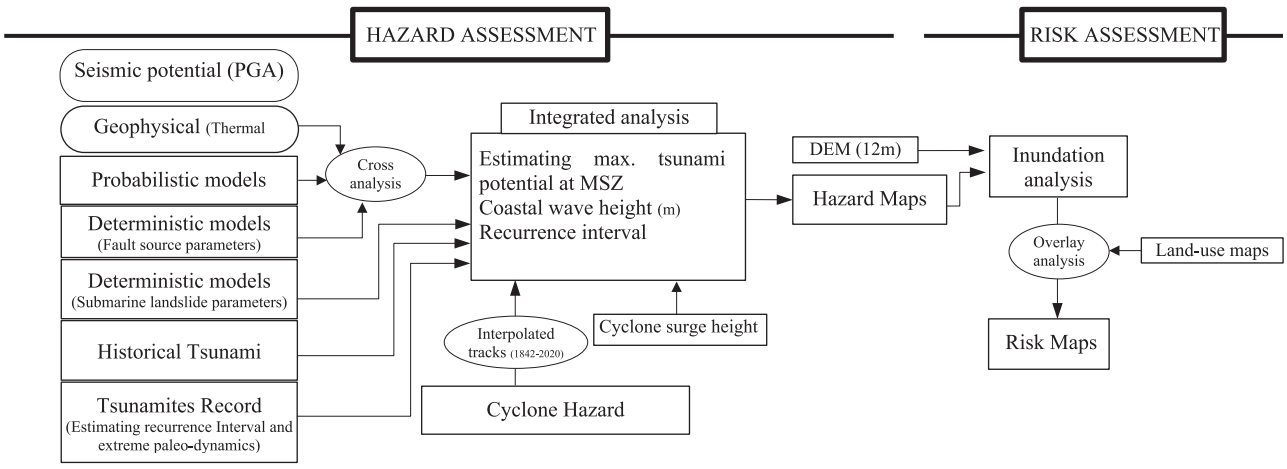

Fig. 3. Flowchart showing sequential order of various processes used for hazard and risk assessment.

ways for this study: 1) the tsunamites record for highest inundation height is reported from the Sur/Fins coast, Oman, which is at nearly equal distance to south of the Makran Coast. The tsunami mechanism for both of these coasts is inferred to be the same as the MSZ. Further, these runup heights are compared with the probabilistic and deterministic models and finally four different wave heights (3, 7, 10, 15 m) for four major cities (Karachi, Gwadar, Ormara and Pasni). Three wave-scenarios under 15 m are also analysed for a possible shorter return period. For inundation analysis, the German Aerospace Center's TanDEM-X 0.4 arcsec digital elevation model (DEM) with a spatial resolution of 12 m is used (see Fig. 4). The TanDEM-X in combination with TerraSAR-X generates DEM from bistatic X-Band interferometric SAR acquisitions. A true or bare ground elevation model or digital terrain model (DTM) is important for setting up the base level for the inundating sea water. The DEM is converted into the DTM by subtracting the approximate heights of the features like plants, houses and poles. The interpolation of open or bare land elevations to buildings, plants, and poles produced the best results for DTM conversion (see Fig. 4). All the processing and analysis are performed in GIS environment using ArcMap 10.6.

The bathtub approach's static nature has the disadvantage of inaccuracy in the estimation of flat, low-lying, and gently rising terrain (Company, 2015), which have been addressed globally in several publications through hydro-morphodynamic numerical modelling especially in the Indian Ocean tsunami 2004 (Prasetya et al., 2011), western Greece (Röbke et al., 2013, Röbke et al., 2015, 2016, 2018), Tohoku, Japan tsunami 2011 (Koshimura et al., 2014), Hilo Bay, Hawaii-Chilean Tsunami 1960 (Liu et al., 1995), German Bight, Germany (Chacón-Barrantes et al., 2013).

4. Results

The results from the multi-proxy approach imply that the MSZ has the potential to trigger ≥Mw 9.0 tsunamigenic earthquake with a recurrence interval between 500 and 1000 years, which may generate a tsunami up to ≥15 m (see Fig. 5 and Table 2). The region south of Pasni is more susceptible to tsunamis due to high seismic activity. In this area, the rigid decollement (Smith et al., 2013), relative geodetic plate motions at Pasni (see Fig. 2) and differential motion(s) between the Sonne fault and MSZ (Kukowski et al., 2000) indicates stress accumulation and release in the area. In this regard, further investigations and evaluation are highly recommended. The seismic and tsunami hazards are very low for a 50-year recurrence interval. The historical record of tsunamis is insufficient and data credibility may be another issue for result validation; however, a compilation of tsunamites bordering the Arabian Sea shows that these events occur every 500 years. For hazard assessment, the estimation of underwater landslides is yet another important milestone to cover, and it has serious implications on the recurrence interval.

The analysis of the cyclonic record since 1958 shows that the intensity and frequency of Category >1 cyclones have increased at an alarming rate (see Fig. 6B). In the last 64 years, the trend trajectory of intensity has raised three intensity levels, from tropical storm (TS) to Category-3. Since 1960, 27 cyclones have been reported, and of these, 14 have developed in the last 7 years. The frequency has increased from 1 cyclone per 10 years from 1960 to 93 to 4 cyclones per 10 years in the following 20 years (1994–2014). The situation has deteriorated further, with two cyclones per year recorded in the last seven years (2015–2021).

The cyclone track density is highest in a linear manner trending north-south at about 250 km in the Arabian Sea west of the Indian Peninsula (see Fig. 6A, B). At this linear patch, the sea surface temperature of ≥27 °C (V. K. Singh and Roxy, 2022) affects the general wind circulation and reduces the vertical wind shear, which aids the development of tropical cyclones (Grey, 1968; Murty, 1984; Zhang and Villarini, 2019; Singh et al., 2020; Hari et al., 2021). Fig. 6B shows three major routes from the main cyclone centre; first leading to Yemen-Oman border and second to cities of Hilf and Muscat and third one leads to India-Pakistan Border region (see Fig. 6B). At times, the cyclones enter the Arabian Sea from the Bay of Bengal and get amplified due to local climatic conditions in the Arabian Sea, as happened in 2007 and 2021. The sea surface temperature of the Arabian Sea has increased by 1.2–1.4 °C in the last four decades, and this rapid rise is attributed to global warming (V. K. Singh and Roxy, 2022). These ocean warmings may continue in the future, and they need to be closely monitored for the cyclone forecast models (Saunders and Lea, 2008; Singh et al., 2020). Most of the population in Gwadar, Pasni, and Ormara lives between 3 and 7 m above sea level and within 1 km of the coast. In these three cities, there are around 0.15 million people. According to rough estimates, 8 million people live between 3 and 15 m above sea level in Karachi. The inundation results for each city are explained separately as follows:

4.1. Gwadar

Gwadar city will bear no damage from the waves as high as 3 m (see Fig. 7). It can only cause minor damage to the ships and boats anchored in the eastern and western bays. The embankments are 4 m from the high tide limit, which would not allow the waves to spill over the population. Waves with a 7 m amplitude have the considerable potential to invade the city. These waves can cause moderate damage to infrastructure and claim human lives. The houses with low RVI will bear severe damage and a 10 m wave scenario will cause serious damage to

Table 2
A- The compilation of various tsunamis with fault source parameters in MSZ and adjoin tectonics. B- The compilation of various tsunamis for landslide source parameters in Arabian Sea.

	Long.	Lat.	Magnitude (Mw)	Azimuth	Length (km)	Width (km)	Water Depth (km)	Epicenter Depth (km)	Moment (N/m)	Min Slip (m)	Max Slip (m)	Avg. Slip (m)	Dip	Rake	Uplift	Wave Height (m)	Software/Code
Hosseini Mehr et al., 2018	24.77	58.8	7.2	270	57	22		10	0.708 × 10*18	0.8	1.8	1.25	7	90	Model not run		SMT
El-Hussain et al., 2018	24.66	65.5	8.8	263	461	110						11	7	90		8	NSWING
	24.55	64.36	8.1	261	150	70						6.6	7	90		3	
M. A. Sarker, 2019	MSZ		8	246	55	70		27				10	7	89		1	MIKE21 Flow
	1945 EQ epicenter		8.4	246	55	70		27				10	7	89		3	Model FM
Saha and Srivastava, 2019	63.48	25.15	8.0	246	150	70		20				7	7	90		3	TSUNAMI-N2
	65.72	25.22	9	250	360	183		20				11	7	90		4	
Heidarzadeh et al., 2008	Jiwani-Pasni-Somiani		8.6	265	500	100		25	1.95 × 10*22			13	7	90		6–9	TSUNAMI-N2
	Jask-Jiwani-Pasni-Somiani		9	265	500	150		25	1.01 × 10*23			25	7	90		12–15	
Heidarzadeh et al., 2009a, 2009b	24.05	63.17	8.1	246	120–150	65–80	2000	27	1.8 × 10*21	5.3	6.6		7	89	1.7–2	Max 7	TSUNAMI-N2, TSUNAMI-N3
Heidarzadeh et al., 2008	25.06	64.01	8.4	240	200	100	50	20	1.8 × 10*21			7.3	6	90	2		TUNAMI-N2,
Heidarzadeh et al., 2007			8	246	Equation Rupture × 0.55			20		Wells and Coppersmith (1994) [25]'s Equation Rupture × 1.187				90		3	
Heidarzadeh and Satake, 2014a				230–260	120–237	40–100		17–30	3 × 10*11 dyn/cm2			6–11	5–9	70–110		5–6	TUNAMI
Rajendran et al., 2008	1945 EQ epicenter		8.1	246	150	70		15				7	7	90		5	TUNAMI-N2,
Okal and Synolakis, 2008	Makran-Pak			265									7	90		2	MOST
	Makran-Pak & Iran			280–265	whole MSZ								7	90		<3	
Jaiswal et al., 2009	24.05	63.90	8.6	270	200	100	2000	30				15	15	90		7	Tunami-N2
Yanagisawa et al., 2009	25	64	8.1	246	40–130	65		15				8–30	7	90		5–10	
Rafi and Mahmood, 2010	1945 EQ epicenter		8.5									5.26				5	MOST
Srivastava et al., 2011	1945 EQ epicenter		9	265	337	190		25				11	7	90		Max 5	TSUNAMI-N2
Arjun et al., 2011	EQ-1945 (as Rastogi)		8.1	270	200	100		30				15	15	90		Max 5	TSUNAMI-N2
Akbarpour Jannat et al., 2011	326 BCE,1008,1897,1945		8.1	280	100–300	50		25					7	89–90		Max 10	ComMIT
Swapna and Srivastava, 2014	61.16	24.59	9	278	366	183		25				11	7	90		3	TUNAMI N2
	66.3	25.20	9	256	366	183		25				11	7	90		4	
	63.48	25.15	8.1	246	150	70		27				7	7	89		2.5	
Payande et al., 2014	1945 EQ epicenter		8.1					25									
	60.5	24.8	7.5					10								4.5	MIKE 21 FM
			8.1					25								8	
			9.1					30								18	
Miranda et al., 2014	Chabhar-Ormara		8.6	268	394	100						8	25	90		Max 4	SW code
	Central Iran MSZ		7.7	286	108	40						3	30	90		Max 0.5	
	Murray Ridge		7.8	49	137	45						3.5	88	180		Max 0.15	

(*continued on next page*)

Table 2 (*continued*)

	Long.	Lat.	Magnitude (Mw)	Azimuth	Length (km)	Width (km)	Water Depth (km)	Epicenter Depth (km)	Moment (N/m)	Min Slip (m)	Max Slip (m)	Avg. Slip (m)	Dip	Rake	Uplift	Wave Height (m)	Software/Code
Rehman et al., 2015	63.01	24.72	7–8.5	276	100–150	50		7.62				0.01–2.63	3	90		Max 1.9	ComMIT
Suppasri et al., 2016	MSZ		9.0		900	150						25				18	TUNAMI
			8.6		500	100						13				10	
			8.3		55	80						8.5				6	
			8.3		55	70						4.3–10				6	
Delavar et al., 2017	1945 EQ epicenter		8.1	246	130	70	2000	27	1.8 × 10*21			6.6	7	89	2	5	ComMIT
			8.1	270	130	70			1.8 × 10*21			15		90		10	
Rashidi et al., 2018a	Iranian Makran		9	280	400	150		25	1.01 × 10*23			25	7	90		10	COMCOT
			7.7	286	108	40	1000			3			30	90		2	
			7.8	49	137	45	1000			3.5			88			3	
Rashidi et al., 2018a, 2018b			9					25	4.5 × 10*22					88		23	

B	Longitude	Latitude	Bulk Density (kg/m^3)	Viscosity (m/s^2)	Initial Submergence (Travel Distance) (m)	Water Depth (m)	Seabed Slope (degree)	Volume (km^3)	Slide length (km)	Slide Thickness (m)	Slide width (km)	Wave Height (m)	Software/ Code
Rodriguez et al., 2013	60.27	17.2		25 to 500		2000		40		140		2.5	AVALANCHE
Rastgoftar and Soltanpour, 2016	64.1	24.75			1134		6		15	500	10	Max 18–20	TOPICS and FUNWAVE
Suppasri et al., 2016	Persian Gulf					Coastal landslides		1	20	5	10	<1	TUNAMI
								0.5	10	5	10	<1	
Heidarzadeh and Satake, 2014a, 2014b, 2017	63	24.8	2150		1000–2000	1300–2000		45		600		29.9	TUNAMI-N2
			2150		1000–2000	1300–2000			20	600	20	15.2	
			2150		1000–2000	1300–2000			20	800	20	23.7	
Salmanidou et al., 2019	67.06	23.1	2000		500–2000	250–450				100–300	6–10.5	Max 2	JAGURS
Baptista et al., 2020	61.6	24.4					5					0.2	
Nouri, M., 2020	58.75	23.87					25	4	4.5	600	4	24	COMCOT

Table 5
The compilation of tsunamites discovered at different coasts along the Arabian Sea (sorted age-wise).

No.	Event Year (radiometric)	Event Assigned	Location	Brief detail	Reference
1	1948 ± 9 to 1969 ± 10 (Back as of 2022)	1945	Pindara to Okha, India	The documented sand-sheet in the paleo mud flats shows physical, geochemical and biological characteristics such as basal erosional/sharp contact with the underlying unit and lack of sorting along with the presence of mud-clasts. The sedimentary layer also shows an abnormal inland extent of >570 m from the present high-water line.	(Prizomwala et al., 2022)
2	1945[a] Tsunamigenic earthquake event	1945		In this study, particle size, stable isotopic and foraminiferal (taxa and taphonomy) analyses were conducted on surface sediment samples from Sur Lagoon to determine modern spatial trends in the lagoon for future comparison with over-wash sediments deeper in the geologic record	(Pilarczyk and Reinhardt, 2012)
3	Older than 1958 [b]	1945	Sur Lagoon,	5-25 cm thick bed of bivalve shell taphonomy	(Donato et al., 2008)
4	C^{14} 722–905 cal BP	1000	Oman	They reinterpreted the age of 25-cm-thick tsunamigenic layer based on the new discovery of parallel-oriented woody axes in the sedimentological context of the tsunami shell layer in the Sur lagoon. The woody axes were analysed anatomically and identified as pertaining to the grey mangrove Avicennia.	(Decker et al., 2022)
6	1508–1681 CE	1524	Kelshi, India	This laterally extending 30–40-cm-thick tsunamites zone, coinciding with a habitation level, displays varied sedimentary structures including scour-fill features, and is inter-layered with shells, at a height of 3 m from the high-tide level.	(Rajendran et al., 2020)
7	C^{14} - ~ 872 BP OSL – (Ka) (1130 ± 170) (1110 ± 160)	1000	Fins to Tiwi, Oman	Sedimentological and archaeological evidence for past tsunamis and describe new data on the impact of the 1945 Makran tsunami in Oman.	(Hoffmann et al., 2020)
8	C^{14} - (BP) (1565 ± 35)(1930 ± 30) (950 ± 30) (1445 ± 30) OSL – (Ka) (1.11 ± 0.11) (1.18 ± 0.11) (1.29 ± 0.22)	1000	Panjor to Luni, India	Sedimentology and geochemistry reveal an offshore origin of this sand sheet, from where it was eroded by a high energy wave and deposited in a supratidal environment	(Prizomwala et al., 2018)
9	OSL – (1.3 ± 0.3) (6.6 ± 0.7) (35.4 ± 4.3)	1052	Mundra-Bhadreshwar, Madhavpur-Chorwad, Ratiya, India	GPR studies and trenching the subsurface sand layers shows features that identify and locate features that might have formed during a reported extreme event and its effects. a wave height of ~4–5 m along Saurashtra coast. Southern Owen Ridge is considered as tsunami source.	(Bhatt et al., 2016)
10	4522 ± 200 BP	4522	Ras ul Hadd, Oman	Archaeologically rich evidence of past extreme wave events is preserved in the onshore stratigraphic record. Comprehensive mapping and analysis of extreme wave deposits suggests an Early Bronze Age.	(Hoffmann et al., 2015)
11	5840 ± 30 BP	5840	Fins, Oman	Investigated coarse- to fine- grained, marine tsunami deposits using GPR. Wedging out of sediments and fining inland features, as well as several erosion features at the base of the deposit. Minimum calculated runup height of >17 m.	(Koster et al., 2014)
12			Ramin, Iran	The boulders, weighing up to 18 t, are found up to 6 m above present mean sea level and up to 40 m from the present shoreline.	(Shah-Hosseini et al., 2011)
13			Dive Agar, India	Sediment signatures at the two nearby beach sites on the west Two sedimentary	(Sangode and Meshram, 2013)
14			Guhagar, India	deposits are inferred as indicative of two palaeo tsunami events relating to the Sunda Arc in the south and the Makran tectonic zone in the north. The occurrence of sporadic boulders, wedge- shaped heavy mineral sand layers and capping of the deposit by a pedogenic surface at Guhagarh depicts an older tsunami of larger magnitude compared to Dive Agar.	
15			Fins to Sur, Oman	The blocks occur as individual rocks of up to 120 tons, as imbricated sets and as "boulder trains	(Hoffmann et al., 2013a, 2013b)

[a] Age based on foraminiferal provenance and taphonomy.
[b] Age Based on Pb ^{210} ($n = 1$). Sample immediately above the tsunamites.

the city. Along with inundating the city centre, it will also inundate the area planned for future industry (see Fig. 7). The ≥15 m scenario creates total havoc in the city as the tombolo neck will completely submerge under the water. According to interviews of the 1945 tsunami survivors, Shado, Moulla, and Khuda towns were inundated by the 1945 Tsunami. So, it can be inferred that waves height then were at least ≥4 m high at the eastern bay of Gwadar. The beach topography at Gwadar is greatly altered by the construction of embankments on both sides of the bays, which reduces the efficacy of a comparative analysis with the 1945 tsunami.

4.2. Pasni

The effect of a 3 m high wave in Pasni is almost the same as that of Gwadar, but it has the potential for minor damage to the infrastructure along the beach (see Fig. 8 in the supplements). The waves up to 7 m height will have serious consequences on the town as about one third of the town submerges under the water (see Fig. 8 in the supplements). The submerged area also partly includes the densely populated city centre. It will block the major road that links Pasni to the rest of the country. The 10 m wave height has the potential to inundate the entire city centre, including Wadasar, Parag and partly Shol. In this scenario, infrastructure and human life will suffer greatly. Almost the entire town will be affected in the 15-min scenario. At the city centre, single-story buildings will be approximately 7–10 m under water. The 1945 tsunami (12 m) comparative inundation analysis fits well with our results in Pasni, except there is a sand accretion of 500 m at the northern port area and a ~ 3 m high and 2.5 km long concrete barrier built at the southern port area. These barriers provide some coastal defence against the waves, especially those related to cyclones.

4.3. Ormara

Most of the population resides below 6 m elevation within 1 km of

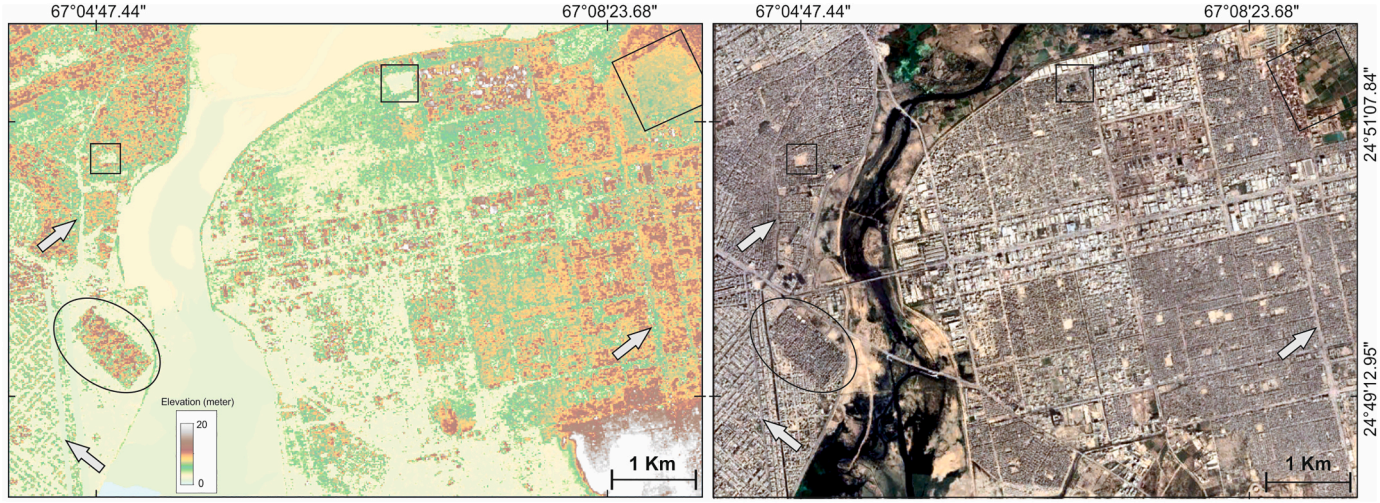

Fig. 4. A comparison of the DEM (left) and a satellite image (right) of a section of Karachi. The buildings in the oval circle show the roof-top elevations as compared with the ground elevations in the surroundings. The arrows and squares point to the few ground elevation sites (roads, open lands) in between the densely populated areas used for the DTM interpolation.

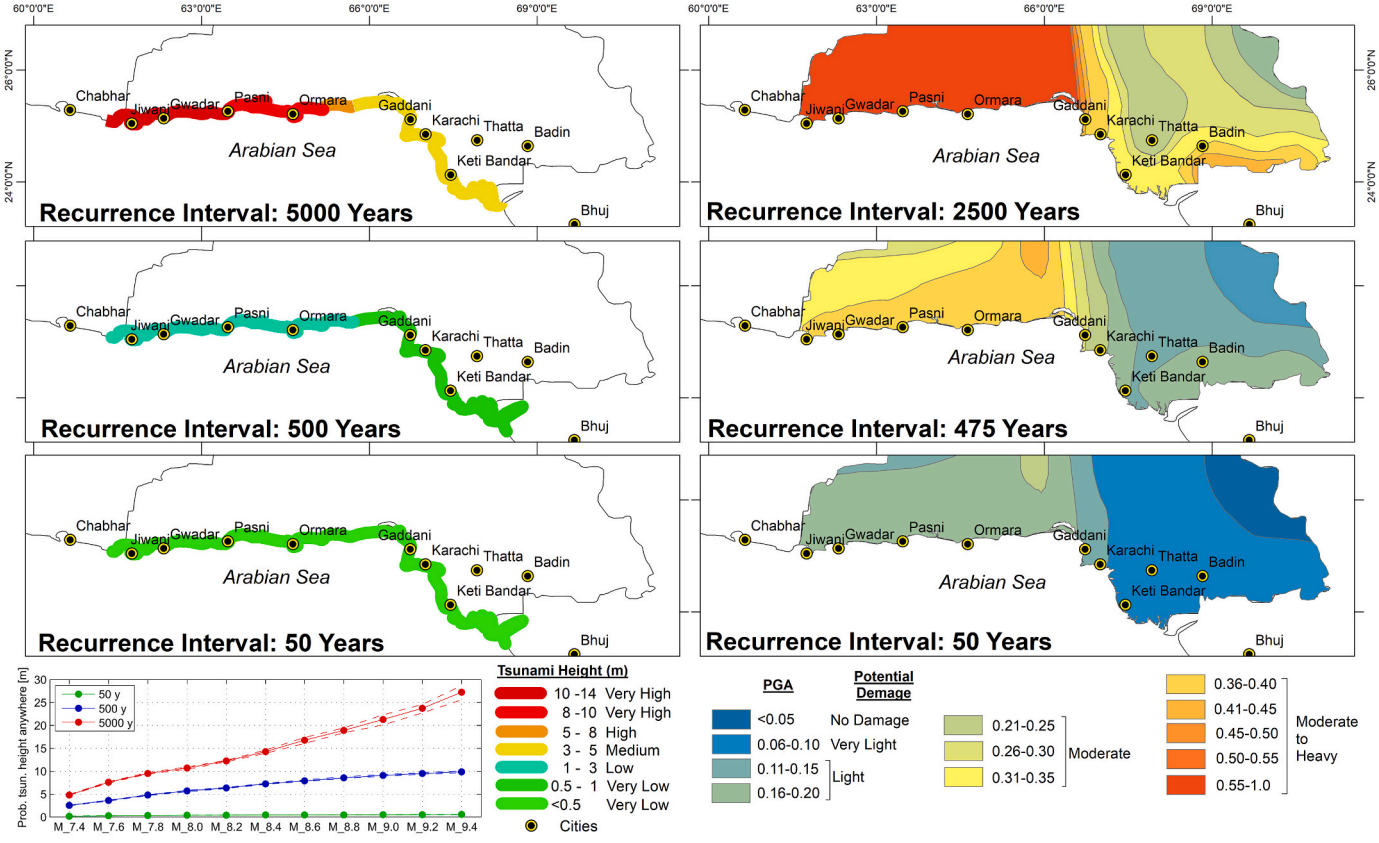

Fig. 5. The left column shows probabilistic tsunami heights with different recurrence intervals by Hoechner et al. (2016). The right column shows the seismic hazard maps based on probabilistic peak ground acceleration (PGA) for different recurrence intervals by Ahmed et al. (2019). The probability of tsunami height is calculated from the instrumental and historical seismicity at the MSZ.

the eastern and western bays (see Fig. 9 in the supplements). In the 3 m scenario, the city undergoes minor damage to the houses along the beach, especially at the eastern bay. A 7 m tsunami wave has the potential to seriously affect the town. As estimated from the interviews of the 1945 tsunami survivors, approximately a 7 m wave affected the town. In this regard, a 10 m wave and a 15 m wave have a potential to affect the whole town with 4 m and 9 m flow depths respectively. Also, along with city, the hammer head's neck (tombolo) will completely submerge under the water.

4.4. Karachi

Karachi is the biggest city along the Makran Coast and is highly vulnerable to the extreme waves. Though the evaluated hazard potential

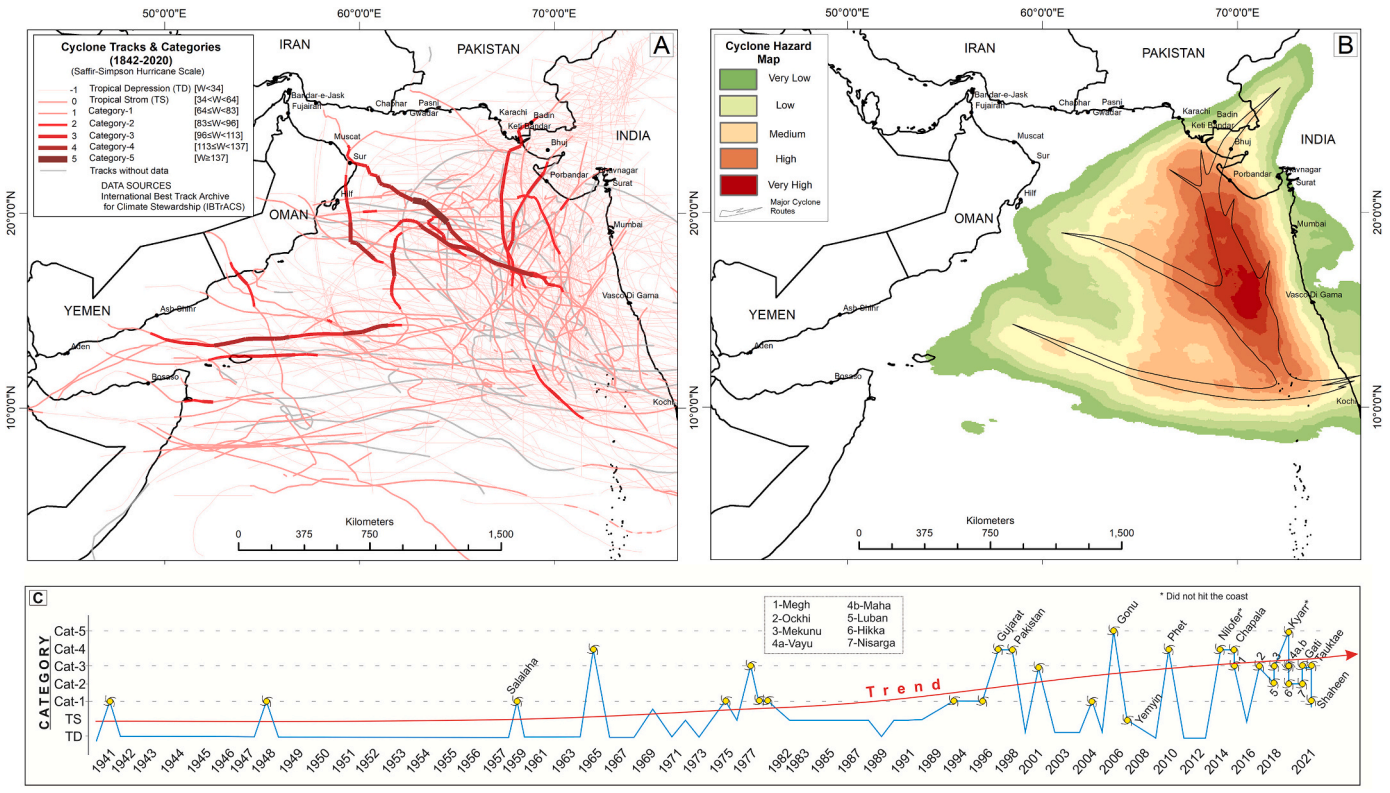

Fig. 6. A. Cyclone tracks in the Arabian Sea since 1842 (International Best Track Archive for Climate Stewardship IBTrACS, 2020). The segmented colour scheme shows the cyclone category. B. Cyclone hazard map based on the cyclone density. The branched structure shows the high frequency cyclone routes. C. graph shows a trend in the frequency and intensity of cyclones.

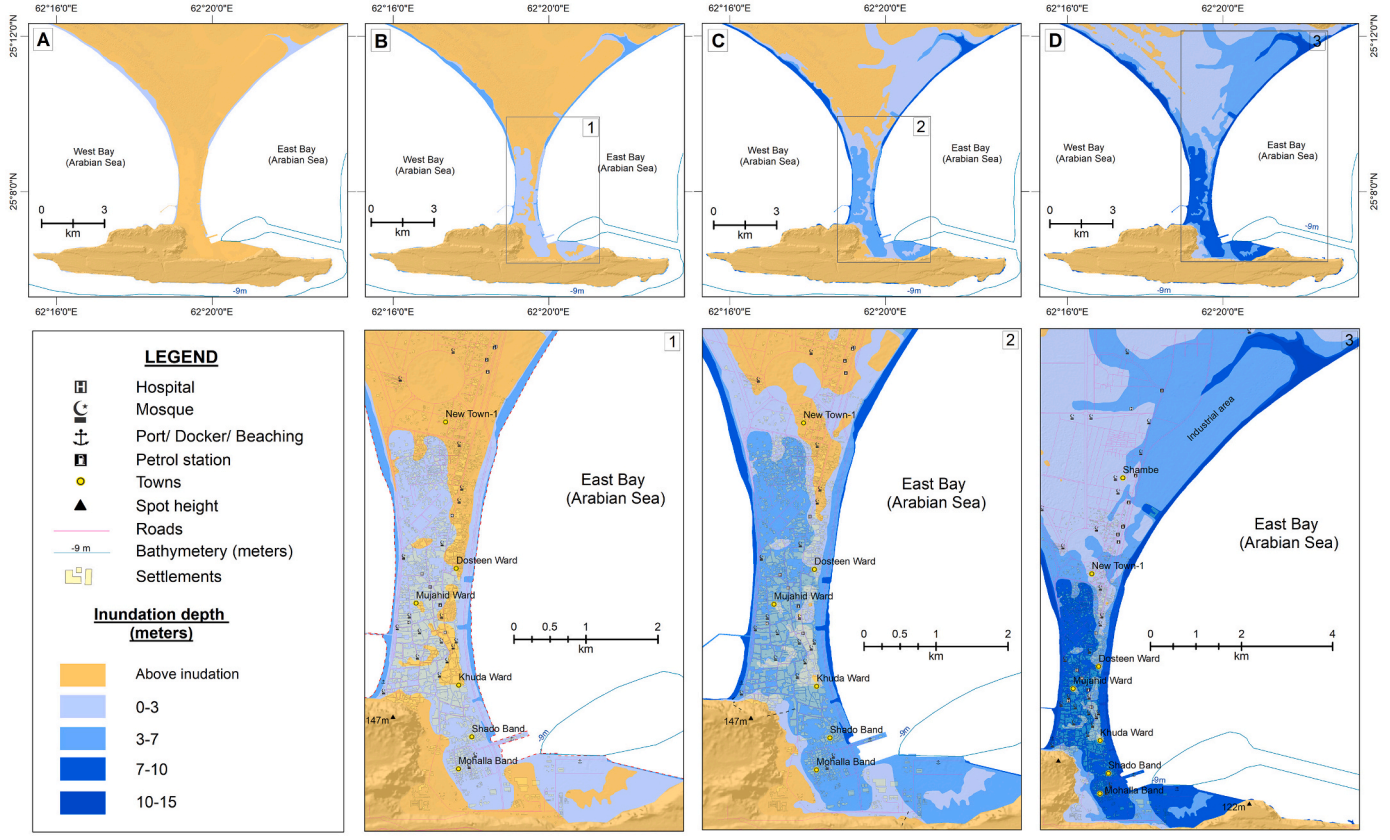

Fig. 7. Results of inundation analyses for Gwadar. A. 3 m scenario B. 7 m scenario C. 10 m scenario D. 15 m scenario.

for such extreme waves is low except for tsunamigenic landslide hazard. 3 m waves have a minor impact on Jamali, Clifton, the Monara-Bundal islands, and the Defence Housing Authority (DHA). The 7 m and 10 m waves will have serious consequences due to their higher tendency to inundate deep into the city (see Fig. 10 in the supplements). Other than directly facing the shoreline, the creeks (Layari, Ghizri, Chinna) provide main pathways for a deep and far inland inundation; therefore, proximity to these creeks is at high risk (see Fig. 10). Waves of 15 m can cause significant loss of life and infrastructure damage. The Monora and Bundal islands will be submerged for >10 m in this scenario. Overcrowding, substandard buildings, proximity to the beach, and a poor economic situation increase the risk factor and reduce the society's resilience. Karachi has an advantage over the other cities in that it has many multi-story concrete buildings, which may provide a quick vertical evacuation during such an event.

5. Discussion

The establishment of the maximum tsunami potential is essential for its hazard and risk assessment. In this regard, each approach has its own limitations, particularly gaps in knowledge, data and different computational types. As compared to a single proxy, the synergy of five proxies has improved the level of information and confidence in the hazard estimation and risk assessment. In comparative analysis for a scenario, the proxies either validate or negate and in some cases, narrow down the result range. The probability studies based on various techniques and methods estimate the recurrence interval of a mega tsunami event between 2500 and 5000 years. These probable models only take earthquake sources into account and do not consider other non-seismic tsunami sources. In this regard, considering the well-studied tsunami events of 1945 CE and 1000 CE in the northern Arabian Sea, the recurrence interval narrows down to 1000 years. With these two arguments, a quick and crude analysis implies that non-seismic tsunami sources and/or cascading sources (co-seismic landslides) generate about 40% to 80% of tsunamis in the Arabian Sea. This ratio is high, so we keep the interpretation tentative. Globally, about 80% of tsunamis have an earthquake source (Harbitz et al., 2014; Løvholt, 2017; Behrens et al., 2021). Non-seismic tsunami sources, particularly underwater landslides, complicate hazard assessment in terms of magnitude and recurrence interval. In comparison to an earthquake, a landslide has a greater potential for larger wave heights due to its large vertical slip (see Table 2B). However, the size of triggered mass characterizes the tsunami size. The 1945 (major) and 2013 (minor) tsunamis in the Arabian Sea are also attributed to a submarine landslide triggered by offshore and terrestrial earthquakes, respectively. These recent tsunami events also reflect the high frequency of underwater slope failures (Hoffmann et al., 2014; Heidarzadeh and Satake, 2017). Landslide stability is dependent on several geotechnical and lithological factors (slope angle, consolidation, specific gravity, density, particle type and size, consistency limits, and compaction). Many agents can lower the threshold of these factors, especially earthquakes, submarine volcanic activity, marine life, and submarine anthropogenic activities like communication cables, mining, and drilling. Considering moderate to high-scale offshore earthquakes ($Mw \geq 6.5$) capable of destabilising a mega submarine landslide, the frequency of slope failures should be high because the $Mw \geq 6.5$ occurs every 20 years (Table 3 in the supplements) and provides critical landslides that have completed or are near the completion of their angle of repose (Heidarzadeh et al., 2008). The landslide-related hazard is an important research gap, which greatly hampers the tsunami hazard assessment. The precise measurement and monitoring of these factors to estimate their slip rates and failure times is a mammoth task.

The compilation shows the sequence of events as 1945 CE, 1524 CE, 1000 CE, 4522 ± 200 BP and 5840 ± 200 BP (Table 5). The interval between the first three clusters of events is about 500 years, while the fourth and fifth clusters have an interval of 1100 years, but there is a gap of >3000 years between these two clusters of events. This huge interval (3000 years) has three possible speculations: First, there was no such extreme wave event and if the event(s) occurred, either they could not be preserved in the sedimentary record or, if preserved, they have not been discovered yet. This approach has limitations: 1) Pakistan's coast lines, which are highly susceptible to tsunamigenic earthquakes and have yet to be explored for palaeotsunami deposits that could enrich Table 5. 4) the status of interpretation for most of these as tsunamites is tentative and not proven yet, as their deposition by other non-seismic tsunami sources and cyclones is not completely ruled out. 3) Date approximation, geological inferences and assumptions, and the correlation of an extreme wave event with a previously known event, such as the 1000 CE tsunami.

For Karachi, the inundation analysis and risk results are quite complex to conclude. The complexity is due to the city's tightly packed nature and the confusing historic extreme wave record. In the tightly packed areas, DEM could not resolve the streets, roads, and roof tops in some areas. The maximum wave height expected for this city is due to its location, as the high-intensity waves generated at MSZ mostly propagate in a north-south direction, and the city lies exactly to the east of MSZ. However, the deterministic models show that Karachi expects about half of the maximum wave height recorded at the Ormara. It is the easternmost city, located in a northerly direction from MSZ, and is the closest to Karachi of the three. If we apply this hypothesis to the 1945 tsunami waves, the maximum wave height calibrated and estimated at Ormara was about 4 m (Kakar et al., 2014). The calibration is based on claims made by 1945 tsunami survivors that Ormara city rose approximately 2 m after the earthquake (Page et al., 1979; Kakar et al., 2014). Page et al. (1979), along with interviewing senior citizens, provided field evidence of a 2 m uplift. In Karachi, wave height was about 2–3 m as reported by the 1945 tsunami survivors (Kakar et al., 2014), but Karachi's 1945 tide gauge record shows a 52 cm waveform (Neetu et al., 2011). Taking this hypothesis ahead for the Mw 9.0 (25 m slip) earthquake at MSZ. It could generate a maximum wave height of 18 m at Ormara and 9 m at Karachi's Coast. The nuclear power plant near Karachi is at least 15 m high from the high tide limit. Through the above discussion, we may conclude that this part of the study area is not likely to receive waves higher than 9 m. However, its vulnerability with reference to a mega-landslide needs evaluation.

The Makran Coast, due to its proximity to the MSZ could not benefit much from the far-field early warning system, namely the Indian Ocean Tsunami Warning and Mitigation System (IOTWS) installed in the Arabian Sea. With reference to a tsunami generated at MSZ, this system is beneficial for the south-western Indian Coast, including Mumbai city, as its far-field warning mechanism can work for it. Numerical modelling of 1945 tsunamigenic earthquake (Mw 8.1) shows that the tsunami reaches at Pasni, Karachi and Deep-Ocean Assessment and Reporting of Tsunami stations (DART) station in about 15, 100 and 60 min respectively (Heidarzadeh et al., 2007). There is a reaction time of 40 min for alert issuance and evacuation. The Pakistan Meteorological Department (PMD) is the focal agency for monitoring coastal hazards and issuing warning alerts. PMD established a near-field tsunami early warning system in 2010 and a well-established cyclone early warning system in the 1960s. Even so, the tsunami reaction time (15 min) at the nearest coast is extremely short. On the resilience and preparedness side, the large number of casualties and property losses during the cyclones of 1998, 1999, 2007, 2010 and 2021 reflect a dejected level of preparedness and resilience and for tsunamis the level is even more pathetic.

6. Conclusions

This study includes a hazard and risk assessment of tsunamis and cyclones along the Makran Coast of Pakistan. The highly populated Karachi (~20 million), newly developed economic zone at Gwadar and nuclear power plant along the coast have heightened the focus of the topic. We used five approaches including probabilistic, deterministic, geophysical, sedimentary and historical analysis to estimate the wave

potential in the Arabian Sea and constructed four different wave scenarios for inundation analysis. Inundation scenarios were performed in a GIS environment coupled with land use maps to demarcate the areas at high and very high risk.

Results indicate very high risk at Ormara, Pasni and Gwadar due to their orientation, low topography and proximity to the tsunami source. However, a 3 m scenario will not have a significant impact on the Gwadar due to barriers (4 m) created by newly constructed highways on both sides (see Fig. 7). Karachi is the most vulnerable city to extreme waves due to population pressure, substandard buildings, proximity to the beach, and a poor economic situation that increase the risk factor and reduce the society's resilience. However, its position with respect to the MSZ and propagating waves needs to be studied in detail. Furthermore, the nuclear power plant near Karachi is at least 15 m above the high tide line and is therefore safe, provided its other components, like the cooling systems, keep on working during the extreme wave event (see Fig. 10 in the supplements). Overall, the inundation analysis shows that the damage to the Makran Coast will be minor for 3 m, moderate for 7 m and severe for the 10–15 m and higher tsunamis, especially for the four major cities discussed in the paper. In these four cities, at least 0.7 million people are at risk. Aside from tsunami hazard, the intensity and frequency of cyclones since 1958 have increased significantly, from Tropical Storm to Category-3 with two cyclones per year respectively. The enormous number of lives and property losses during the cyclones in 1998, 1999, 2007, 2010, and 2021 reflect a disheartening level of preparedness and resilience, and the level is even more pitiful in the case of tsunamis.

6.1. Outlook

The coastline along the high tsunami hazard zone (Gwadar to Ormara) should be investigated for field evidence (tsunamites) to foster the palaeo-tsunami record to estimate source potential and the recurrence interval. The active seismic zone south of Pasni in relation to the Sonne Fault, the nature of the decollement basement and the slow GPS velocity at Pasni should be investigated in detail. Submarine landslide potential is poorly known, but detailed bathymetric studies may help in determining the potential. Further, the high hazard zones demarcated in the studies may be revisited at regular intervals to estimate the slip rate and time of slope failure. Though the forecasting side of cyclones has greatly improved with time, the resilience and preparedness aspects are still far from satisfactory. The estuaries of Ormara and Pasni are suitable sites for mangrove forestation. The Karachi Beach (Clifton) may be turned into artificial estuaries that may serve the purpose of planting a mangrove forest. Along with many other benefits, it may act as a coastal defence structure against the extreme waves. There is a considerable scientific understanding of the earthquake and tsunami dynamics, but still there are large data and knowledge gaps, assumptions and uncertainties. Due to these shortcomings and limitations, the timing and exact location of earthquakes and tsunamis are still unpredictable (Behrens et al., 2021). Till there is a scientific breakthrough, the option in hand is to get well prepared by enhancing the community awareness and resilience.

Authors contributions

RH constructed the idea, planned the methodology, interpreted the results, and then reached conclusions. SA assisted in data interpretation and writing process. GH co-supervised the process. KR supervised the whole process and provided technical, environmental, financial, and personal support for the research work.

Financial support

The research work is generously supported by the German Academic Exchange Service (DAAD) (Research Grants-Doctoral Programme no. 57507871).

Declaration of Competing Interest

The authors declare that they have no known competing financial interests or personal relationships that could have appeared to influence the work reported in this paper.

The authors declare the following financial interests/personal relationships which may be considered as potential competing interests:

Rashid Haider reports financial support was provided by German Academic Exchange Service (DAAD).

Data availability

All historical documents and newspaper accounts that the paper refers to can be found at https://iotic.ioc-unesco.org/ (IOTIC, 2021). The 12 m digital elevation model data is owned and protected by the German Aerospace Center.

Acknowledgement

We are grateful to the German Aerospace Center for providing the unprocessed digital elevation model data (TanDEM-X, DEM 12 m) for the inundation analysis.

Appendix A. Supplementary data

Supplementary data to this article can be found online at https://doi.org/10.1016/j.margeo.2023.107032.

References

Ahmed, M., Lodi, S.H., Rafi, M.M., 2019. Probabilistic seismic hazard analysis based zoning map of Pakistan. J. Earthq. Eng. 1–36 https://doi.org/10.1080/13632469.2019.1684401.

Akbarpour Jannat, M.R., Noranian Esfahani, M., Chegini, V., Rezanejad, K., 2011. Hazards associated with tsunami waves in the gulf of Oman. J. Coast. Res. 865–869.

Ali, K.F., De-Boer, D.H., 2008. Factors controlling specific sediment yield in the upper Indus River basin, northern Pakistan. Hydrol. Process. 2274, 2267–2274. https://doi.org/10.1002/hyp.

Arjun, S., Kalarani, K., Dhanya, P., Praveen, S.S., Reshmi, A.K., Kurian, N.P., Murthy, M. V.R., Hameed, T.S.S., Prakash, T.N., 2011. Numerical simulation of the 1945 Makran tsunami on the southwest coast and Lakshadweep islands of India. Mar. Geod. 34, 68–76. https://doi.org/10.1080/01490419.2011.547801.

ArRajehi, A., McClusky, S., Reilinger, R., Daoud, M., Alchalbi, A., Ergintav, S., Gomez, F., Sholan, J., Bou-Rabee, F., Ogubazghi, G., Haileab, B., Fisseha, S., Asfaw, L., Mahmoud, S., Rayan, A., Bendik, R., Kogan, L., 2010. Geodetic constraints on present-day motion of the Arabian Plate: Implications for Red Sea and Gulf of Aden rifting. Tectonics 29, 1–10. https://doi.org/10.1029/2009TC002482.

Banghar, A., Syke, L.R., 1981. Focal mechanism of an earthquake from the Southern Ocean. Tectonophysics 79, 37–41.

Baptista, M.A., Miranda, J.M., Omira, R., El-Hussain, I., 2020. Study of the 24 September 2013 Oman Sea tsunami using linear shallow water inversion. Arab. J. Geosci. 13 https://doi.org/10.1007/s12517-020-05632-z.

Behrens, J., Løvholt, F., Jalayer, F., Lorito, S., Salgado-Gálvez, M.A., Sørensen, M., Abadie, S., Aguirre-Ayerbe, I., Aniel-Quiroga, I., Babeyko, A., Baiguera, M., Basili, R., Belliazzi, S., Grezio, A., Johnson, K., Murphy, S., Paris, R., Rafliana, I., De Risi, R., Rossetto, T., Selva, J., Taroni, M., Del Zoppo, M., Armigliato, A., Bureš, V., Cech, P., Cecioni, C., Christodoulides, P., Davies, G., Dias, F., Bayraktar, H.B., González, M., Gritsevich, M., Guillas, S., Harbitz, C.B., Kânoğlu, U., Macías, J., Papadopoulos, G.A., Polet, J., Romano, F., Salamon, A., Scala, A., Stepinac, M., Tappin, D.R., Thio, H.K., Tonini, R., Triantafyllou, I., Ulrich, T., Varini, E., Volpe, M., Vyhmeister, E., 2021. Probabilistic tsunami hazard and risk analysis: a review of research gaps. Front. Earth Sci. 9, 1–28. https://doi.org/10.3389/feart.2021.628772.

Bell, K.C., 2011. Lessons from the Reconstruction of Post-Tsunami Aceh: Build Back Better Through Ensuring Women are at the Center of Reconstruction of Land and Property. © World Bank, Washington, DC.

Berryman, K., 2005. Review of Tsunami Hazard and Risk in New Zealand. Inst. Geol. Nucl, Sci, p. 139.
Bhatt, N., Murari, M.K., Ukey, V., Prizomwala, S.P., Singhvi, A.K., 2016. Geological evidences of extreme waves along the Gujarat coast of western India. Nat. Hazards 84, 1685–1704. https://doi.org/10.1007/s11069-016-2507-6.
Bourget, J., Zaragosi, S., Ellouz-Zimmermann, S., Ducassou, E., Prins, M.A., Garlan, T., Lanfumey, V., Schneider, J.L., Rouillard, P., Giraudeau, J., 2010. Highstand vs. lowstand turbidite system growth in the Makran active margin: Imprints of high-frequency external controls on sediment delivery mechanisms to deep water systems. Mar. Geol. 274, 187–208. https://doi.org/10.1016/j.margeo.2010.04.005.
Byrne, D.E., Sykes, L.R., Davis, D.M., 1992. Great thrust earthquakes and aseismic slip along the plate boundary of the Makran Subduction Zone. J. Geophys. Res. 97, 449–478.
Chacón-Barrantes, S., Narayanan, R.R.A., Mayerle, R., 2013. Several Tsunami Scenarios at the North Sea and their Consequences at the German Bight.
Clift, P.D., Giosan, L., 2014. Sediment fluxes and buffering in the post-glacial Indus Basin. Basin Res. 26, 369–386. https://doi.org/10.1111/bre.12038.
Company, K.A., 2015. Comparing the " Bathtub Method " with MIKE21 HD Flow Model for Modelling Storm Surge Inundation - Case Study Kiel Fjord.
Cornell, C.A., Vanmarcke, E.H., 1969. The major influences on seismic risk. In: Proceedings of the Fourth World Conference on Earthquake Engineering, pp. 69–83.
De Martini, P.M., Bruins, H.J., Feist, L., Goodman-Tchernov, B.N., Hadler, H., Lario, J., Mastronuzzi, G., Obrocki, L., Pantosti, D., Paris, R., Reicherter, K., Smedile, A., Vött, A., 2021. The Mediterranean Sea and the Gulf of Cadiz as a natural laboratory for paleotsunami research: recent advancements. Earth-Sci. Rev. 216, 103578 https://doi.org/10.1016/j.earscirev.2021.103578.
Decker, V., Gee, C.T., Schucht, P.J., Lindauer, S., Hoffmann, G., 2022. Life on the Edge : A Powerful Tsunami Overwhelmed Indian Ocean Mangroves Life on the Edge : A Powerful Tsunami Overwhelmed Indian Ocean Mangroves One Millennium Ago. https://doi.org/10.3390/f13060922.
Delavar, M.R., Mohammadi, H., Sharifi, M.A., Pirooz, M.D., 2017. Tsunami risk assessment modelling in Chabahar port, Iran. Int. Arch. Photogramm. Remote Sens. Spat. Inf. Sci. - ISPRS Arch. 42, 461–467. https://doi.org/10.5194/isprs-archives-XLII-2-W7-461-2017.
Donato, S.V., Reinhardt, E.G., Boyce, J.I., Rothaus, R., Vosmer, T., 2008. Identifying tsunami deposits using bivalve shell taphonomy. Geology 36, 199–202. https://doi.org/10.1130/G24554A.1.
Donato, S.V., Reinhardt, E.G., Boyce, J.I., Pilarczyk, J.E., Jupp, B.P., 2009. Particle-size distribution of inferred tsunami deposits in Sur Lagoon, Sultanate of Oman. Mar. Geol. 257, 54–64. https://doi.org/10.1016/j.margeo.2008.10.012.
El-Hussain, I., Omira, R., Al-Habsi, Z., Baptista, M.A., Deif, A., Mohamed, A.M.E., 2018. Probabilistic and deterministic estimates of near-field tsunami hazards in northeast Oman. Geosci. Lett. 5 https://doi.org/10.1186/s40562-018-0129-4.
Ellouz, N., Lallemant, S.J., Castilla, R., Mouchot, N., Leturmy, P., Battani, A., Buret, C., Cherel, L., Desaubliaux, G., Deville, E., Ferrand, J., Lügcke, A., Mahieux, G., Mascle, G., Mühr, P., Pierson-Wickmann, A.-C., Robion, P., Schmitz, J., Danish, M., Hasany, S., Shahzad, A., Tabreez, A., 2007. Offshore frontal part of the Makran Accretionary prism: The Chamak Survey (Pakistan). In: Thrust Belts and Foreland Basins, Frontiers in Earth Sciences. https://doi.org/10.1007/978-3-540-69426-7_18.
Fournier, M., Patriat, P., Leroy, S., 2001. Reappraisal of the Arabia-India-Somalia triple junction kinematics. Earth Planet. Sci. Lett. 189, 103–114. https://doi.org/10.1016/S0012-821X(01)00371-5.
Fournier, M., Chamot-Rooke, N., Petit, C., Fabbri, O., Huchon, P., Maillot, B., Lepvrier, C., 2008. In situ evidence for dextral active motion at the Arabia-India plate boundary. Nat. Geosci. 1, 94–98. https://doi.org/10.1038/ngeo.2007.24.
Fournier, M., Chamot-Rooke, N., Rodriguez, M., Huchon, P., Petit, C., Beslier, M.O., Zaragosi, S., 2011. Owen Fracture Zone: The Arabia-India plate boundary unveiled. Earth Planet. Sci. Lett. 302, 247–252. https://doi.org/10.1016/j.epsl.2010.12.027.
Frank, N.L., Husain, S.A., 1971. The Deadliest Tropical Cyclone in History. Bull. Am. Meteorol. Soc. 52, 438–445. https://doi.org/10.1175/1520-0477(1971)052<0438:tdtcih>2.0.co;2.
Gandhi, D., Chavare, K.A., Prizomwala, S.P., Bhatt, N., Bhatt, N.Y., Mohan, K., Rastogi, B. K., 2017. Testing the numerical models for boulder transport through high energy marine wave event: An example from southern Saurashtra, western India. Quat. Int. 444, 209–216. https://doi.org/10.1016/j.quaint.2016.05.021.
Gordon, R.G., Demets, C., 1989. Present-day motion along the Owen fracture zone and Dalrymple trough in the Arabian Sea. J. Geophys. Res. 94, 5560–5570. https://doi.org/10.1029/JB094iB05p05560.
Grando, G., McClay, K., 2007. Morphotectonics domains and structural styles in the Makran accretionary prism, offshore Iran. Sediment. Geol. 196, 157–179. https://doi.org/10.1016/j.sedgeo.2006.05.030.
Griffin, J., Latief, H., Kongko, W., Harig, S., Horspool, N., Hanung, R., Rojali, A., Maher, N., Fuchs, A., Hossen, J., Upi, S., Edi Dewanto, S., Rakowsky, N., Cummins, P., 2015. An evaluation of onshore digital elevation models for modeling tsunami inundation zones. Front. Earth Sci. 3, 1–16. https://doi.org/10.3389/feart.2015.00032.
Harbitz, C.B., Løvholt, F., Bungum, H., 2014. Submarine landslide tsunamis: How extreme and how likely? Nat. Hazards 72, 1341–1374. https://doi.org/10.1007/s11069-013-0681-3.
Hari, V., Pathak, A., Koppa, A., 2021. Dual response of Arabian Sea cyclones and strength of Indian monsoon to Southern Atlantic Ocean. Clim. Dyn. 56, 2149–2161. https://doi.org/10.1007/s00382-020-05577-9.
Heidarzadeh, M., Satake, K., 2014a. Possible sources of the tsunami observed in the northwestern Indian ocean following the 2013 September 24 Mw 7.7 Pakistan inland earthquake. Geophys. J. Int. 199, 752–766. https://doi.org/10.1093/gji/ggu297.
Heidarzadeh, M., Satake, K., 2014b. New Insights into the Source of the Makran Tsunami of 27 November 1945 from Tsunami Waveforms and Coastal Deformation Data. Pure Appl. Geophys. 172, 621–640. https://doi.org/10.1007/s00024-014-0948-y.
Heidarzadeh, M., Satake, K., 2017. A combined earthquake-landslide source model for the tsunami from the 27 november 1945 Mw 8.1 makran earthquake. Bull. Seismol. Soc. Am. 107, 1033–1040. https://doi.org/10.1785/0120160196.
Heidarzadeh, M., Pirooz, M.D., Mokhtari, M., Zaker, N.H., 2007. Modeling of tsunami propagation in the vicinity of the southern coasts of Iran. Int. J. Civ. Eng. 5, 223–234. https://doi.org/10.1115/OMAE2007-29082.
Heidarzadeh, M., Pirooz, M.D., Zaker, N.H., Yalciner, A.C., Mokhtari, M., Esmaeily, A., 2008. Historical tsunami in the Makran Subduction Zone off the southern coasts of Iran and Pakistan and results of numerical modeling. Ocean Eng. 35, 774–786. https://doi.org/10.1016/j.oceaneng.2008.01.017.
Heidarzadeh, M., Pirooz, M.D., Zaker, N.H., 2009a. Modeling the near-field effects of the worst-case tsunami in the Makran subduction zone. Ocean Eng. 36, 368–376. https://doi.org/10.1016/j.oceaneng.2009.01.004.
Heidarzadeh, M., Pirooz, M.D., Zaker, N.H., Yalciner, A.C., 2009b. Preliminary estimation of the tsunami hazards associated with the Makran subduction zone at the northwestern Indian Ocean. Nat. Hazards 48, 229–243. https://doi.org/10.1007/s11069-008-9259-x.
Hoechner, A., Babeyko, A.Y., Zamora, N., 2016. Probabilistic tsunami hazard assessment for the Makran region with focus on maximum magnitude assumption. Nat. Hazards Earth Syst. Sci. 16, 1339–1350. https://doi.org/10.5194/nhess-16-1339-2016.
Hoffmann, G., Reicherter, K., 2014. Reconstructing Anthropocene extreme flood events by using litter deposits. Glob. Planet. Chang. 122, 23–28. https://doi.org/10.1016/j.gloplacha.2014.07.012.
Hoffmann, G., Reicherter, K., Wiatr, T., Grützner, C., 2011. Evidence For Holocene Tsunami-Impact Along the Shoreline of Oman. 2nd INQUA-IGCP-567. Int. Work. Act. Tectonics, Earthq. Geol. Archaeol. Eng. 88–91.
Hoffmann, G., Reicherter, K., Wiatr, T., Grützner, C., Rausch, T., 2013a. Block and boulder accumulations along the coastline between Fins and Sur (Sultanate of Oman): Tsunamigenic remains? Nat. Hazards 65, 851–873. https://doi.org/10.1007/s11069-012-0399-7.
Hoffmann, G., Rupprechter, M., Al Balushi, N., Grützner, C., Reicherter, K., 2013b. The impact of the 1945 Makran tsunami along the coastlines of the Arabian Sea (Northern Indian Ocean) – a review. Z. Geomorphol. Suppl. Issues 57, 257–277. https://doi.org/10.1127/0372-8854/2013/s-00134.
Hoffmann, G., Al-Yahyai, S., Naeem, G., Kociok, M., Grützner, C., 2014. An Indian Ocean tsunami triggered remotely by an onshore earthquake in Balochistan, Pakistan. Geology 42, 883–886. https://doi.org/10.1130/G35756.1.
Hoffmann, G., Grützner, C., Reicherter, K., Preusser, F., 2015. Geo-archaeological evidence for a Holocene extreme flooding event within the Arabian Sea (Ras al Hadd, Oman). Quat. Sci. Rev. 113, 123–133. https://doi.org/10.1016/j.quascirev.2014.09.033.
Hoffmann, G., Grützner, C., Schneider, B., Preusser, F., Reicherter, K., 2020. Large Holocene tsunamis in the northern Arabian Sea. Mar. Geol. 419 https://doi.org/10.1016/j.margeo.2019.106068.
Hosseini Mehr, A., Maleki Asayesh, B., Mokhtari, M., 2018. Splay Faults in the Makran Subduction Zone and Changes of their Transferred Coulomb Stress. J. Earth Sp. Phys. 43, 1–10. https://doi.org/10.22059/jesphys.2017.61703.
Jaiswal, R.K., Singh, A.P., Rastogi, B.K., 2009. Simulation of the Arabian Sea Tsunami propagation generated due to 1945 Makran Earthquake and its effect on western parts of Gujarat (India). Nat. Hazards 48, 245–258. https://doi.org/10.1007/s11069-008-9261-3.
Kakar, D.M., Naeem, G., Usman, A., Hasan, H., Lohdi, H.A., Srinivasalu, S., Andrade, V., Rajendran, C.P., Beni, A.N., Hamzeh, M.A., Hoffmann, G., 2014. Elders recall an earlier tsunami on Indian Ocean shores. EOS Trans. Am. Geophys. Union 95, 485–486.
Kalsi, S.R., Gupta, M., 2003. Success and failure of early warning systems: A case study of the Gujarat Cyclone of June, 1998. In: Zschau, J., Küppers, A. (Eds.), Early Warning Systems for Natural Disaster Reduction. Springer, Berlin Heidelberg, Berlin, Heidelberg, pp. 199–202. https://doi.org/10.1007/978-3-642-55903-7_26.
Khaledzadeh, M., Ghods, A., 2022. Estimation of size of megathrust zone in the Makran subduction system by thermal modelling. Geophys. J. Int. 228, 1530–1540. https://doi.org/10.1093/gji/ggab417.
Khan, S.A., Shah, M.A., Qaisar, M., 2003a. Seismic risk analysis of coastal area of Pakistan. Acta Seismol. Sin. English Ed. 16, 382–394. https://doi.org/10.1007/s11589-003-0071-0.
Khan, S.A., Shah, M.A., Qaisar, M., 2003b. Seismic risk analysis of coastal area of Pakistan. Acta Seismol. Sin. English Ed. 16, 382. https://doi.org/10.1007/s11589-003-0071-0.
Khan, M.A., Bendick, R., Bhat, M.I., Bilham, R., Kakar, D.M., Khan, S.F., Lodi, S.H., Qazi, M.S., Singh, B., Szeliga, W., Wahab, A., 2008. Preliminary geodetic constraints on plate boundary deformation on the western edge of the Indian plate from TriGGnet (Tri-University GPS Geodesy Network). J. Himal. Earth Sci. 41, 71–87.
Knapp, K.R., Kruk, M.C., Levinson, D.H., Diamond, H.J., Neumann, C.J., 2010. The international best track archive for climate stewardship (IBTrACS). Bull. Am. Meteorol. Soc. 91, 363–376. https://doi.org/10.1175/2009BAMS2755.1.
Kopp, C., Fruehn, J., Flueh, E.R., Reichert, C., Kukowski, N., Bialas, J., Klaeschen, D., 2000. Structure of the makran subduction zone from wide-angle and reflection seismic data. Tectonophysics 329, 171–191. https://doi.org/10.1016/S0040-1951(00)00195-5.
Koshimura, S., Hayashi, S., Gokon, H., 2014. The impact of the 2011 Tohoku earthquake tsunami disaster and implications to the reconstruction. Soils Found. 54, 560–572. https://doi.org/10.1016/j.sandf.2014.06.002.

Koster, B., Hoffmann, G., Grützner, C., Reicherter, K., 2014. Ground penetrating radar facies of inferred tsunami deposits on the shores of the Arabian Sea (Northern Indian Ocean). Mar. Geol. 351, 13–24. https://doi.org/10.1016/j.margeo.2014.03.002.
Kukowski, N., Schillhorn, T., Flueh, E.R., Huhn, K., 2000. Newly identified strike-slip plate boundary in the northeastern Arabian Sea. Geology 28, 355–358.
Kukowski, N., Schillhorn, T., Huhn, K., Von Rad, U., Husen, S., Flueh, E.R., 2001. Morphotectonics and mechanics of the central Makran accretionary wedge off Pakistan. Mar. Geol. 173, 1–19. https://doi.org/10.1016/S0025-3227(00)00167-5.
Laane, J.L., Chen, W.-P., 1989. The Makran earthquake of 1983 April 18: A possible analogue to the Puget Sound earthquake of 1965. Geophys. J. Int. 98, 1–9.
Latcharote, P., Al-Salem, K., Suppasri, A., Pokavanich, T., Toda, S., Jayaramu, Y., Al-Enezi, A., Al-Ragum, A., Imamura, F., Anawat, K.A., 2018. Tsunami hazard evaluation for Kuwait and Arabian Gulf due to Makran Subduction Zone and Subaerial landslides. Nat. Hazards 93, 127–152. https://doi.org/10.1007/s11069-017-3097-7.
Liu, P.L.F., Cho, Y.S., Yoon, S.B., Seo, S.N., 1995. Numerical Simulations of the 1960 Chilean Tsunami Propagation and Inundation at Hilo, Hawaii, 99–115. https://doi.org/10.1007/978-94-015-8565-1_7.
Løvholt, F., 2017. Tsunami Hazard and Risk Assessment. United Nations Off. Disaster Risk Reduct, pp. 1–9.
Mahmood, N., Khan, K., Rafi, Z., Lovholt, D.F., 2012. Mapping of Tsunami Hazard along Makran Coast of Pakistan 1–39.
Masuda, M., Williams, C., Shahkarami, A., Rafique, F., Bryngelson, J., 2012. Tsunami Vulnerability Function Development Based on the 2011 Tohoku Earthquake in Japan. In: 15 World Conf. Earthq. Eng.
Milliman, J.D., Syvitski, J.P.M., 1992. Geomorphic/tectonic control of sediment discharge to the ocean: the importance of small mountainous rivers. J. Geol. 100, 525–544. https://doi.org/10.1086/629606.
Miranda, J.M., Baptista, M.A., Omira, R., 2014. On the use of Green's summation for tsunami waveform estimation: A case study. Geophys. J. Int. 199, 459–464. https://doi.org/10.1093/gji/ggu266.
Mouchot, N., Loncke, L., Mahieux, G., Bourget, J., Lallemant, S., Ellouz-Zimmermann, N., Leturmy, P., 2010. Recent sedimentary processes along the Makran trench (Makran active margin, off Pakistan). Mar. Geol. 271, 17–31. https://doi.org/10.1016/j.margeo.2010.01.006.
Murty, T.S., 1984. Storm surges-Meteorological Ocean Tides. Bull. Fish. Res. Board Canada, p. 898.
Neetu, S., Suresh, I., Shankar, R., Nagarajan, B., Sharma, R., Shenoi, S.S.C., Unnikrishnan, A.S., Sundar, D., 2011. Trapped waves of the 27 November 1945 Makran tsunami: Observations and numerical modeling. Nat. Hazards 59, 1609–1618. https://doi.org/10.1007/s11069-011-9854-0.
Okal, E.A., Synolakis, C.E., 2008. Far-field tsunami hazard from mega-thrust earthquakes in the Indian Ocean. Geophys. J. Int. 172, 995–1015. https://doi.org/10.1111/j.1365-246X.2007.03674.x.
Page, W.D., Alt, J.N., Cluff, L.S., Plafker, G., 1979. Evidence for the recurrence of large-magnitude earthquakes along the makran coast of Iran and Pakistan. Tectonophysics 52, 533–547. https://doi.org/10.1016/B978-0-444-41783-1.50081-7.
Pagnoni, G.I., Armigliato, A., Tinti, S., 2021. Estimation of human damage and economic loss of buildings related to tsunami inundation in the city of augusta, italy. Geol. Soc. Spec. Publ. 501, 327–342. https://doi.org/10.1144/SP501-2019-134.
Payande, A.R., Niksokhan, M.H., Naserian, H., 2014. Tsunami hazard assessment of Chabahar bay related to megathrust seismogenic potential of the Makran subduction zone. Nat. Hazards 76, 161–176. https://doi.org/10.1007/s11069-014-1476-x.
Pedgley, D.E., 1967. Cyclones along the Along Arabian Coast. Weather.
Pendse, C.G., 1946. The Mekran Earthquake of the 28th November 1945. Sci. Notes X 141–146.
Pilarczyk, J.E., Reinhardt, E.G., 2012. Testing foraminiferal taphonomy as a tsunami indicator in a shallow arid system lagoon: Sur, Sultanate of Oman. Mar. Geol. 295–298, 128–136. https://doi.org/10.1016/j.margeo.2011.12.002.
Pilarczyk, J.E., Reinhardt, E.G., Boyce, J.I., Schwarcz, H.P., Donato, S.V., 2011. Assessing surficial foraminiferal distributions as an overwash indicator in Sur Lagoon, Sultanate of Oman. Mar. Micropaleontol. 80, 62–73. https://doi.org/10.1016/j.marmicro.2011.06.001.
Platt, J.P., Leggett, J.K., Young, J., Raza, H., Alam, S., 1985. Large-scale sediment underplating in the Makran accretionary prism, southwest Pakistan. Geology 13, 507–511. https://doi.org/10.1130/0091-7613(1985)13<507:LSUITM>2.0.CO;2.
Prasetya, G., Borrero, J., de Lange, W., Black, K., Healy, T., 2011. Modeling of inundation dynamics on Banda Aceh, Indonesia during the great Sumatra tsunamis December 26, 2004. Nat. Hazards 58, 1029–1055. https://doi.org/10.1007/s11069-010-9710-7.
Prins, M.A., Postma, G., Cleveringa, J., Cramp, A., Kenyon, N.H., 2000. Controls on terrigenous sediment supply to the Arabian Sea during the late quaternary: The Indus fan. Mar. Geol. 169, 327–349. https://doi.org/10.1016/S0025-3227(00)00086-4.
Prizomwala, S.P., Gandhi, D., Ukey, V.M., Bhatt, N., Rastogi, B.K., 2015. Coastal boulders as evidences of high-energy marine events from Diu Island, west coast of India: storm or palaeotsunami? Nat. Hazards 75, 1187–1203. https://doi.org/10.1007/s11069-014-1371-5.
Prizomwala, S.P., Gandhi, D., Bhatt, N.N., Winkler, W., Kumar, M.R., Makwana, N., Bhatt, N.N., 2018. Geological evidence for AD 1008 tsunami along the Kachchh coast, Western India: Implications for hazard along the Makran Subduction Zone. Sci. Rep. 8, 1–8. https://doi.org/10.1038/s41598-018-35193-x.
Prizomwala, S.P., Tandon, A., Joshi, N., Makwana, N., 2021. Reconstructing the catalogue for extreme wave events from the Gujarat coastline (Western India) and their implications to coastal settlers during the last 6000 years. Quat. Int. 599–600, 24–31. https://doi.org/10.1016/j.quaint.2021.03.004.
Prizomwala, S.P., Vedpathak, C., Tandon, A., Das, A., Makwana, N., Joshi, N., 2022. Geological footprints of the 1945 Makran tsunami from the west coast of India. Mar. Geol. 446, 106773 https://doi.org/10.1016/j.margeo.2022.106773.
Quittmeyer, R.C., Kafka, A.L., 1984. Constraints on plate motions in southern Pakistan and the northern Arabian Sea from the focal mechanisms of small earthquakes. J. Geophys. Res. 89, 2444–2458.
Quittmeyer, R.C., Farah, A., Jacob, H.K., 1979. The seismicity of Pakistan and its relation to surface faults. In: Farah, A., Dejong, K.A. (Eds.), Geodynamics of Pakistan. Geological Survey of Pakistan, Quetta, pp. 271–284.
Rafi, Z., Mahmood, N., 2010. Tsunami Inundation for Potential Earthquake at Makran Subduction Zone. Tech. Rep. No. PMD-45/2010.
Rajendran, C.P., Ramanamurthy, M.V., Reddy, N.T., Rajendran, K., 2008. Hazard implications of the late arrival of the 1945 Makran tsunami. Curr. Sci. 95, 1739–1743.
Rajendran, C.P., Heidarzadeh, M., Sanwal, J., Karthikeyan, A., Rajendran, K., 2020. The Orphan Tsunami of 1524 on the Konkan Coast, Western India, and Its Implications. Pure Appl. Geophys. https://doi.org/10.1007/s00024-020-02575-0.
Rashidi, A., Shomali, Z.H., Dutykh, D., Keshavarz Faraj Khah, N., 2018a. Evaluation of tsunami wave energy generated by earthquakes in the Makran subduction zone. Ocean Eng. 165, 131–139. https://doi.org/10.1016/j.oceaneng.2018.07.027.
Rashidi, A., Shomali, Z.H., Keshavarz Farajkhah, N., 2018b. Tsunami simulations in the Western Makran using hypothetical heterogeneous source models from World's Great Earthquakes. Pure Appl. Geophys. 175, 1325–1340. https://doi.org/10.1007/s00024-018-1842-9.
Rashidi, A., Shomali, Z.H., Dutykh, D., Keshavarz Farajkhah, N., 2020. Tsunami hazard assessment in the Makran subduction zone. Nat. Hazards 100, 861–875. https://doi.org/10.1007/s11069-019-03848-1.
Rastgoftar, E., Soltanpour, M., 2016. Study and numerical modeling of 1945 Makran tsunami due to a probable submarine landslide. Nat. Hazards 83, 929–945. https://doi.org/10.1007/s11069-016-2356-3.
Rehman, K., Jadoon, T., Hussain, M., Ahmad, Z., Ali, Aamir, Ali, Asghar, Ahmed, S., 2015. Tsunamigenic analysis in and around makran. J. Earthq. Eng. 19, 332–355. https://doi.org/10.1080/13632469.2014.982835.
Reilinger, R., McClusky, S., Vernant, P., Lawrence, S., Ergintav, S., Cakmak, R., Ozener, H., Kadirov, F., Guliev, I., Stepanyan, R., Nadariya, M., Hahubia, G., Mahmoud, S., Sakr, K., ArRajehi, A., Paradissis, D., Al-Aydrus, A., Prilepin, M., Guseva, T., Evren, E., Dmitrotsa, A., Filikov, S.V., Gomez, F., Al-Ghazzi, R., Karam, G., 2006. GPS constraints on continental deformation in the Africa-Arabia-Eurasia continental collision zone and implications for the dynamics of plate interactions. J. Geophys. Res. Solid Earth 111, 1–26. https://doi.org/10.1029/2005JB004051.
Röbke, B.R., Vött, A., Willershäuser, T., Fischer, P., Hadler, H., 2015. Considering coastal palaeogeographical changes in a numerical tsunami model - A progressive base to compare simulation results with field traces from three coastal settings in western Greece. Z. Geomorphol. 59, 157–188. https://doi.org/10.1127/zfg-suppl/2014/S-00210.
Röbke, B.R., Schüttrumpf, H., Vött, A., 2016. Effects of different boundary conditions and palaeotopographies on the onshore response of tsunamis in a numerical model - A case study from western Greece. Cont. Shelf Res. 124, 182–199. https://doi.org/10.1016/j.csr.2016.04.010.
Röbke, B.R., Schüttrumpf, H., Vött, A., 2018. Hydro- and morphodynamic tsunami simulations for the ambrakian gulf (Greece) and comparison with geoscientific field traces. Geophys. J. Int. 213, 317–339. https://doi.org/10.1093/gji/ggx553.
Rodriguez, M., Fournier, M., Chamot-Rooke, N., Huchon, P., Bourget, J., Sorbier, M., Zaragosi, S., Rabaute, A., 2011. Neotectonics of the Owen Fracture Zone (NW Indian Ocean): Structural evolution of an oceanic strike-slip plate boundary. Geochem. Geophys. Geosyst. 12 https://doi.org/10.1029/2011GC003731.
Rodriguez, M., Fournier, M., Chamot-Rooke, N., Huchon, P., Zaragosi, S., Rabaute, A., 2012. Mass wasting processes along the Owen Ridge (Northwest Indian Ocean). Mar. Geol. 326–328, 80–100. https://doi.org/10.1016/j.margeo.2012.08.008.
Rodriguez, M., Chamot-Rooke, N., Hébert, H., Fournier, M., Huchon, P., 2013. Owen Ridge deep-water submarine landslides: Implications for tsunami hazard along the Oman coast. Nat. Hazards Earth Syst. Sci. 13, 417–424. https://doi.org/10.5194/nhess-13-417-2013.
Saha, S., Srivastava, K., 2019. Tsunami simulation along the south west coast of India: Lakshadweep Islands acting as wave-barricade. Indian J. Geo-Marine Sci. 48, 1640–1647.
Salaree, A., Okal, E.A., 2015. Field survey and modelling of the Caspian Sea tsunami of 1990 June 20. Geophys. J. Int. 201, 621–639. https://doi.org/10.1093/gji/ggv044.
Salmanidou, D.M., Heidarzadeh, M., Guillas, S., 2019. Probabilistic Landslide-Generated Tsunamis in the Indus Canyon, NW Indian Ocean. Using Statistical Emulation. Pure Appl. Geophys. 176, 3099–3114. https://doi.org/10.1007/s00024-019-02187-3.
Sangode, S.J., Meshram, D.C., 2013. A comparative study on the style of paleotsunami deposits at two sites on the west coast of India. Nat. Hazards 66, 463–483. https://doi.org/10.1007/s11069-012-0542-5.
Sarker, M.A., 2019. Numerical modelling of tsunami in the Makran Subduction Zone–A case study on the 1945 event. J. Oper. Oceanogr. 12, S212–S229. https://doi.org/10.1080/1755876X.2018.1527883.
Saunders, M.A., Lea, A.S., 2008. Large contribution of sea surface warming to recent increase in Atlantic hurricane activity. Nature 451, 557–560. https://doi.org/10.1038/nature06422.
Schneider, B., Hoffmann, G., Reicherter, K., 2016. Scenario-based tsunami risk assessment using a static flooding approach and high-resolution digital elevation data: An example from Muscat in Oman. Glob. Planet. Chang. 139, 183–194. https://doi.org/10.1016/j.gloplacha.2016.02.005.

Shah-Hosseini, M., Morhange, C., Naderi Beni, A., Marriner, N., Lahijani, H., Hamzeh, M., Sabatier, F., 2011. Coastal boulders as evidence for high-energy waves on the Iranian coast of Makran. Mar. Geol. 290, 17–28. https://doi.org/10.1016/j.margeo.2011.10.003.

Singh, V.K., Roxy, M.K., 2022. A review of ocean-atmosphere interactions during tropical cyclones in the north Indian Ocean. Earth-Sci. Rev. 226, 103967 https://doi.org/10.1016/j.earscirev.2022.103967.

Singh, V.K., Roxy, M.K., Deshpande, M., 2020. The unusual long track and rapid intensification of very severe cyclone Ockhi. Curr. Sci. 119, 771–779. https://doi.org/10.18520/cs/v119/i5/771-779.

Smart, G.M., Crowley, K.H.M., Lane, E.M., 2016. Estimating tsunami run-up. Nat. Hazards 80, 1933–1947. https://doi.org/10.1007/s11069-015-2052-8.

Smith, G.L., McNeill, L., Henstock, I.J., Bull, J., 2012. The structure and fault activity of the Makran accretionary prism. J. Geophys. Res. 117, 1–17. https://doi.org/10.1029/2012JB009312.

Smith, G.L., McNeill, L.C., Wang, K.H., He, Jiangheng, Henstock, T.J., 2013. Thermal structure and megathrust seismogenic potential of the Makran subduction zone. Geophys. Res. Lett. 40, 1528–1533. https://doi.org/10.1002/grl.50374.

Srivastava, K., Dimri, V.P., Swaroopa Rani, V., Krishna Kumar, R., Narain, L., 2011. Would makran Tsunami skip Mumbai, India? no it would reach 8 minutes later than Ratnagiri. Indian J. Geo-Marine Sci. 40, 620–623.

Suppasri, A., Latcharotel, P., Pokavanich, T., Al-Salem, K., Al-Enezi, A., Toda, S., Imamura, F., 2016. Tsunami Hazard Assessment for the Arabian Gulf from Earthquakes and Surface Landslides. J. Japan Soc. Civ. Eng. Ser. B2. https://doi.org/10.2208/kaigan.72.i_1675. Coastal Eng. 72, I_1675-I_1680.

Swapna, M., Srivastava, K., 2014. Effect of Murray ridge on the tsunami propagation from Makran subduction zone. Geophys. J. Int. 199, 1430–1441. https://doi.org/10.1093/gji/ggu336.

Tarbotton, C., Dominey-Howes, D., Goff, J.R., Papathoma-Kohle, M., Dall'osso, F., Turner, I.L., 2012. GIS-based techniques for assessing the vulnerability of buildings to tsunami: current approaches and future steps. Geol. Soc. Spec. Publ. 361, 115–125. https://doi.org/10.1144/SP361.10.

Vaziri, S.H., Reinhart, E.G., Pilarczyk, J.E., 2016. Coastal foraminifera from the Iranian coast of Makran, Oman Sea (Chabahar Bay to Gawater Bay) as an indicator of tsunamis. In: Geological Society of America Annual Meeting. Denver, Colorado, pp. 43–63. https://doi.org/10.22059/geope.2018.255122.648378.

Vernant, P., Nilforoushan, F., Hatzfeld, D., Abbassi, M.R., Vigny, C., Masson, F., Nankali, H., Martinod, J., Ashtiani, A., Bayer, R., Tavakoli, F., Chéry, J., 2004. Present-day crustal deformation and plate kinematics in the Middle East constrained by GPS measurements in Iran and northern Oman. Geophys. J. Int. 157, 381–398. https://doi.org/10.1111/j.1365-246X.2004.02222.x.

Waseem, M., Khan, M.A., Khan, S., 2019. Seismic sources for southern Pakistan and seismic hazard assessment of Karachi. Nat. Hazards 99, 511–536. https://doi.org/10.1007/s11069-019-03755-5.

Waseem, M., Khan, S., Asif Khan, M., 2020. Probabilistic Seismic Hazard Assessment of Pakistan Territory Using an Areal Source Model. Pure Appl. Geophys. 177, 3577–3597. https://doi.org/10.1007/s00024-020-02455-7.

White, R.S., Louden, K.E., 1982. The Makran Continental Margin: Structure of a Thickly Sedimented Convergent Plate Boundary: Convergent Margins: Field Investigations of Margin Structure and Stratigraphy.

Williams, S., Paulik, R., Weaving, R., Bosserelle, C., Chan Ting, J., Wall, K., Simi, T., Scheele, F., 2021. Multiscale quantification of tsunami hazard exposure in a pacific small island developing state: the case of samoa. GeoHazards 2, 63–79. https://doi.org/10.3390/geohazards2020004.

Yanagisawa, H., Koshimura, S., Imamura, F., Watabe, H., Egashira, T., 2009. Tsunami hazard assessment along the coast of Pakistan based on the 1945 Makran tsunami. J. Jpn. Soc. Civ. Eng. Ser. B2. https://doi.org/10.2208/kaigan.65.306. Coastal Eng. B2-65, 306–310.

Yang, X., Qiu, Q., Feng, W., Lin, J., Zhang, J., Zhou, Z., Zhang, F., 2022. Mechanism of the 2017 Mw6.3 Pasni earthquake and its significance for future major earthquakes in the eastern Makran. Geophys. J. Int. 231, 1434–1445. https://doi.org/10.1093/gji/ggac257.

Zafarani, H., Etemadsaeed, L., Rahimi, M., Kheirdast, N., Rashidi, A., Ansari, A., Mokhtari, M., Eskandari-ghadi, M., 2022. Probabilistic tsunami hazard analysis for western Makran, Natural Hazards. Springer, Netherlands. https://doi.org/10.1007/s11069-022-05595-2.

Zhang, W., Villarini, G., 2019. On the role of the Atlantic Ocean in forcing tropic cyclones in the Arabian Sea. Atmos. Res. 220, 120–124. https://doi.org/10.1016/j.atmosres.2019.01.016.